Article

Electroconvulsive therapy generates a hidden wave after seizure

Zachary P Rosenthal[1,*], Joseph B. Majeski[2], Ala Somarowthu[3], Davin K Quinn[4], Britta E. Lindquist[5], Mary E. Putt[6], Antoneta Karaj[6], Chris G Favilla[7], Wesley B. Baker[3], Golkoo Hosseini[8], Jenny P Rodriguez[8], Mario A Cristancho[8,9], Yvette I Sheline[7,8,9,10], C. William Shuttleworth[11], Christopher C. Abbott[4], Arjun G Yodh[2], Ethan M Goldberg[3,7,12]

1. Psychiatry Residency Physician-Scientist Research Track, Perelman School of Medicine, University of Pennsylvania, Philadelphia, PA, USA
2. Department of Physics and Astronomy, University of Pennsylvania, Philadelphia, PA, USA
3. Division of Neurology, Department of Pediatrics, The Children's Hospital of Philadelphia, PA, USA
4. Department of Psychiatry, University of New Mexico School of Medicine, Albuquerque, NM, USA
5. Department of Neurology, University of California San Francisco School of Medicine, San Francisco, CA, USA
6. Department of Biostatistics, Epidemiology & Informatics, Perelman School of Medicine, University of Pennsylvania, Philadelphia, PA, USA
7. Department of Neurology, Perelman School of Medicine, University of Pennsylvania, Philadelphia, PA, USA
8. Department of Psychiatry, Perelman School of Medicine, University of Pennsylvania, Philadelphia, PA, USA
9. Center for Neuromodulation in Depression and Stress, Perelman School of Medicine, University of Pennsylvania, Philadelphia, PA, USA
10. Department of Radiology, Perelman School of Medicine, University of Pennsylvania, Philadelphia, PA, USA
11. Department of Neurosciences, University of New Mexico School of Medicine, Albuquerque, NM, USA
12. Department of Neuroscience, Perelman School of Medicine, University of Pennsylvania, Philadelphia, PA, USA

* Corresponding author

Abstract

Electroconvulsive therapy (ECT) is a fast-acting, highly effective, and safe treatment for medication-resistant depression. Historically, the clinical benefits of ECT have been attributed to generating a controlled seizure; however, the underlying neurobiology is understudied and remains largely unresolved. Using optical neuroimaging to probe neural activity and hemodynamics in a mouse model of ECT, we demonstrated that a second brain event follows seizure: cortical spreading depolarization (CSD). We further found that ECT stimulation pulse parameters and electrode configuration directly shaped the wave dynamics of seizure and subsequent CSD. To translate these findings to human patients, we tested for the presence of hemodynamic signatures of post-ictal CSD using non-invasive diffuse optical monitoring of cerebral blood flow and oxygenation during routine ECT treatments. We found evidence that humans generate hyperemic waves after ECT seizure which are highly consistent with CSD. These results challenge a long-held assumption that seizure is the primary outcome of ECT and point to new opportunities for optimizing ECT stimulation parameters to precisely modulate brain activity and treatment outcomes.

Introduction

Electroconvulsive therapy (ECT) is a life-saving intervention for medication-resistant depression. Treatment consists of electrical pulses delivered to the brain to elicit a controlled (~30-90 second) electrographic seizure while under general anesthesia and muscle relaxants to minimize physical movement. Nearly a century since it was discovered, ECT remains the most clinically effective treatment for severe depression[1]. A typical index course of six to twelve ECT treatments achieves rapid symptom improvement in 60-80% of patients, reducing suicide risk by 50% compared to matched controls who do not receive ECT[2,3]. ECT is also highly effective in mania, psychosis, Parkinson's disease, catatonia, and even status epilepticus – particularly for those with the most severe, medication-resistant symptoms. The procedure is safe and generally well-tolerated, including in pediatric, geriatric, and pregnant populations. Potential risks, such as cognitive slowing or memory impairment, are typically modest compared to improvement in neuropsychiatric symptoms, and resolve when treatment is discontinued. Unfortunately, the proven efficacy and safety of ECT have been overshadowed by stigma and negative portrayal in popular media. As a result, contemporary research on ECT is limited, and the treatment is underutilized[4]. Much could be learned from ECT and the basic physiology underlying its rapid-acting efficacy across a varied range of brain disorders, particularly when modern pharmacology has failed.

For the last eight decades, it has been assumed that seizure is necessary for ECT to elicit clinical improvement[3]. However, not all ECT-induced seizures are therapeutic, and conversely, electrical stimulation below the seizure threshold may also be an effective

treatment[5,6]. The role of seizure in the therapeutic mechanism of ECT is thus uncertain. An important clue to this mechanism may be that ECT induces lasting inhibitory plasticity in brain activity, dampening cortical response to stimulation and reliably reducing propensity for future seizures (i.e., raising the seizure threshold)[7-11]. It has been hypothesized that ECT may elicit inhibitory plasticity through the process of seizure suppression[12], but few studies have explored the cellular, circuit, or network level mechanisms of brain inhibition after ECT.

During ECT, brain activity is typically monitored with a minimal scalp electroencephalography (EEG) montage consisting of two leads on the forehead to measure seizure quality, duration and post-ictal suppression in each hemisphere. However, quantitative seizure metrics from EEG monitoring have shown limited predictive value for ECT clinical outcomes[5-7,13-16]. A great need exists for more robust brain activity biomarkers that can predict treatment efficacy, detect side effects, or guide selection of stimulation parameters. Because ECT electrical pulses saturate the scalp EEG signal, no study has ever measured brain activity during pulse delivery in human patients or animal models. Computational models have helped predict the brain electric field evoked by a single electrical pulse[5,17-19], but there are likely opportunities to further optimize stimulation parameters and improve clinical outcomes using empirical measurements of brain activity during treatment. For example, a seminal randomized controlled trial showed that the choice of two electrode spatial configurations (right unilateral vs. bitemporal), as well as two pulse durations (0.3 vs. 0.5 ms), significantly modulates the clinical efficacy and side effects of ECT[20,21]. The remaining stimulation parameter space

is vast, mostly untested, and with unknown effects on brain activity and clinical outcomes[20]. This includes infinite combinations of pulse properties (duration, frequency, total count, current, polarity, waveform) and electrode spatial configurations. Only three electrode placements have been tested clinically - right unilateral, bitemporal, and bifrontal. There are likely alternative stimulation parameters that would provide superior symptom reduction and lower risk of side effects compared to the current standard-of-care configurations and titration algorithms.

To bridge these knowledge gaps, we employed optical neuroimaging to record brain activity during ECT in both rodent models and human patients. Our data demonstrate that a second brain event follows ECT-induced seizure: cortical spreading depolarization (CSD). In mice, we show that clinically relevant choices of electrode placements and pulse parameters directly modulate the spatial and temporal properties of both seizure and subsequent CSD. We then translate these findings from mice to humans. Using non-invasive diffuse optical monitoring of brain tissue oxygen saturation and blood flow in patients receiving ECT, we find evidence for post-ictal hyperemic waves that are highly consistent with CSD. These discoveries have important implications for ECT's mechanism of action and for optimizing stimulation to target specific brain outcomes.

Methods

Mouse model

All procedures described below were approved by the Institutional Animal Care and Use Committee at the Children's Hospital of Philadelphia in compliance with AAALAC

93 guidelines. Mice were raised in standard cages in a double barrier mouse facility with a
94 12hr-12hr light/dark cycle and *ad libitum* access to food and water. All experiments used
95 n=10 eight-week-old mice (male and female) hemizygous for *Thy1-jRGECO1a* (JAX
96 030525) on a C57BL/6J background, to enable optical imaging of the jRGECO1a
97 fluorescent calcium sensor protein. Pups were genotyped by PCR prior to experiments to
98 confirm the presence of the *Thy1-jRGECO1a* transgene, using the forward primer 5'-
99 ACAGAATCCAAGTCGGAACTC-3' and reverse primer 5'-
100 CCTATAGCTCTGACTGCGTGAC-3'.
101
102 *Cranial window and electrode implantation*
103 Mice were treated preoperatively with subcutaneous buprenorphine-SR (1.0 mg/kg),
104 meloxicam (5.0 mg/kg) and cefazolin (500 mg/kg). Mice were anesthetized with isoflurane
105 (3% induction, 1.5% maintenance). Body temperature was maintained via heating pad.
106 The scalp was shaved, sterilized with alcohol and betadine, incised at midline, and
107 retracted to expose the dorsal skull. Five brass electrode pins with 1.78mm diameter
108 flanges (DigiKey 4443-0-00-15-00-00-03-0) were attached to the intact skull surface using
109 a thin layer of silver conductive epoxy (MG Chemicals 8331D). Electrodes were
110 stereotactically centered relative to bregma (see **Fig. 1a**; #1, frontal: X = 0.00 mm, Y =
111 4.09 mm; #2 and #3, temporo-parietal: X = ±3.40 mm, Y = 0.47 mm; #4 and #5, occipital:
112 X = ±4.69 mm, Y= -4.89 mm). A custom steel headbar was attached to the posterior skull
113 and a cranial window was formed with optically clear dental cement (C&B-Metabond,
114 Parkell Inc., Edgewood, NY). The window was rendered transparent and hardened with

115 clear UV-cure gel nail polish. Animals were allowed to recover from surgery for at least
116 one week prior to imaging.
117
118 *Widefield imaging system*
119 Widefield imaging of neuronal dynamics (jRGECO1a fluorescence) and cerebral
120 hemodynamics (optical intrinsic signal, OIS) was performed using a modified version of
121 a previous method[22], on a Leica M205FA stereoscope fitted with a 0.63× objective to
122 capture the dorsal convexity of the cortex (a ~1 cm^2 area, binned to 128×128 pixels, 0.078
123 mm pixel-width). System optical spectra are depicted in **Extended Data Fig. 1**. White
124 light LED illumination (X-Cite XYLIS) was bandpass filtered to green (525/50 nm,
125 Chroma) and directed through the objective at the cortex. Light reflected and emitted from
126 the brain was then separated into two channels using a 560 nm dichroic and image-
127 splitting optics (Hamamatsu W-VIEW GEMINI). The OIS channel was filtered with a
128 512/25 nm bandpass and attenuated with a 5% transmission neutral density filter
129 (Chroma), optimized to capture light reflectance at the isosbestic point of hemoglobin to
130 approximate total hemoglobin concentration. The jRGECO1a red fluorescence channel
131 was filtered with a 630/92 nm bandpass filter. Both channels were detected side-by-side
132 and spatially co-registered on a single CMOS camera (Hamamatsu ORCA-Flash4.0 V3).
133 An exposure time of 50 ms was used, achieving a sampling rate of 15.7 Hz.
134
135 *Combined imaging and electroconvulsive therapy in mice*
136 Mice were monitored with head-fixed widefield imaging while under dexmedetomidine
137 anesthesia (0.5 mg/kg, IP), which reliably achieved a plane of sedation in ~10 minutes

138 with loss of response to toe-pinch and emergence of anteroposterior ~3 Hz global slow
139 waves that are characteristic of anesthesia[23,24]. ECT pulses were delivered to pairs of
140 cranial electrodes using constant current pulse trains (described below) with an isolated
141 pulse stimulator (A-M Systems 4100). At the end of each recording session, anesthesia
142 was reversed with atipamezole (0.5 mg/kg). Similar to prior reports, seizures were noted
143 to elicit ~1-60 seconds of high amplitude, aperiodic neuronal fluorescence activity globally
144 across the cortex, as well as tonic-clonic limb and tail movements. Several pilot titrations
145 were also conducted using etomidate as well as ketamine/xylazine anesthesia, which
146 likewise demonstrated CSD after ECT seizure (data not shown); dexmedetomidine was
147 ultimately selected because of its hemodynamic safety[25], reversibility, and favorable
148 pharmacodynamic profile as an alpha agonist, avoiding acting directly on GABAergic or
149 glutamatergic currents.
150
151 To broadly survey the stimulation parameter space, n=38 ECT stimulus titrations were
152 performed, each testing a different combination of electrode spatial configuration (5
153 electrodes, 10 possible pairs), frequency (5, 10, 25, 50, 100 Hz) and pulse counts (25,
154 50, 100 pulses); see all tested conditions in **Extended Data Table 1**. All stimulation trials
155 used constant-current, bipolar square waves of 0.5 ms pulse width, similar to routine brief
156 pulse ECT in humans. Within each titration, stimulation was delivered first at 1 mA current
157 and then successively up-titrated to 2 mA, 5 mA, 10 mA, and 25 mA, akin to the
158 individualized low amplitude seizure therapy (ILAST) strategy of ECT[26]. At each current
159 step, brain activity was monitored at baseline for 5 seconds, during stimulation, and then
160 for at least 90s, or until the sustained return of baseline anteroposterior slow waves from

161 anesthesia, before being restimulated at the next highest current step. At the current
162 threshold when seizure elicited CSD, recordings were continued for 10 minutes, and the
163 titration was terminated. Titration sessions within individual mice were spaced at least 1
164 week apart to facilitate washout of acute effects of stimulation.
165
166 To control for effects of resampling the same individuals across titrations with different
167 conditions, mixed effects modeling adjusted for mouse ID. Stimulation conditions were
168 partially randomized and balanced across n=10 mice such that each mouse was treated
169 with multiple frequencies and electrode configurations in varying session order. For any
170 given electrode spatial configuration, multiple frequencies were tested; for each
171 frequency, a mixture of unilateral and bilateral electrode configurations were tested. In
172 n=4 titrations, animals were restimulated one more time to elicit a second CSD – these
173 four secondary CSDs exhibited similar intrinsic amplitude and duration to initial CSDs,
174 and were thus pooled into **Figs. 2a**, **2g**, and **2h** (n=42). Secondary CSDs were excluded
175 from analysis in **Figs. 2f** and **3**. One titration was excluded from analysis because of
176 inadequate head-fixation leading to motion artifact that precluded accurate quantification;
177 it was however visually scored as a right sided CSD and pooled into **Fig. 2f** for
178 completeness (n=39).
179
180 *Mouse widefield optical imaging signal processing*
181 Imaging data were converted into two-channel tiff files. A binary brain mask was manually
182 drawn in MATLAB for each recording; all subsequent analyses were performed on pixels
183 labeled as brain. Image sequences from each mouse (as well as the brain mask for each

184 mouse) were affine-transformed to Paxinos atlas space using the positions of bregma
185 and lambda[27]. A standardized mask of the stimulation electrodes was approximated using
186 Paxinos coordinates (see seizure to electrode distance permutation analysis below).
187 Right and left hemispheric divisions were segmented using a straight line drawn through
188 midline of each image. A dark image with no illumination was subtracted from all frames,
189 and then data were spatially smoothed with a Gaussian filter. The jRGECO1a calcium-
190 sensor fluorescence signal (%dF/F) and total hemoglobin OIS signal (%dA/A) were
191 calculated at each pixel by subtracting and dividing the 20th percentile value from the first
192 4 seconds of baseline (pre-stimulation) raw signal from each recording. The total
193 hemoglobin OIS signal was multiplied by -1 (absorbance) so that positive sign changes
194 indicate increased blood volume/total hemoglobin concentration. Red-shifted
195 fluorophores have significantly reduced hemoglobin absorption artifact compared to
196 green fluorophores[22]. Given that fluorescence %dF/F event peaks were more than an
197 order of magnitude larger than hemoglobin %dA/A changes, we opted not to regress the
198 hemodynamic signal out of the fluorescence signal.
199
200 *Event detection and quantification in neuronal fluorescence data*
201 Optical detection of cortical hemodynamics and calcium dynamics has been extensively
202 cross-validated as a surrogate for routine electrophysiology for detecting CSD, offering
203 rich spatial information about traveling waves.[28-31]. The temporal bounds of seizure and
204 CSD events were identified by taking the derivative of the root mean square of the
205 neuronal fluorescence signal at each pixel. We then used the MATLAB function
206 'findchangepts' to find abrupt signal changes at the start and end of seizure and CSD

events. We used an event detection threshold of %dF/F signal rising greater than 20% of baseline. Note, typical widefield %dF/F (fluorescence change) values are +/- 5-10% during routine physiological fluctuations in a mouse. In contrast, seizure and CSD are such large events that %dF/F fluorescence typically rises by 50-200%. The event detection threshold of 20% was determined through trial and error to accurately identify the bounds of seizure and CSD. This approach was cross-validated against the current gold standard for electrographic CSD detection - visual scoring by a trained clinician[32]. Recordings (and pixels therein) not crossing this threshold were excluded from analysis. For each event (seizure or CSD) in each pixel, duration was calculated as the difference between start and end times, and amplitude was calculated as the peak %dF/F value between the start and end time. Then, average event amplitude was computed within right hemisphere, left hemisphere, and total brain space by averaging across pixels. Overall event durations were computed by comparing the event start times in the first and last pixel with right hemisphere, left hemisphere, and total brain space. For CSDs, the first pixel within the brain mask to have an event start time was used as a global reference point for computing time to peak at other pixels for spatial maps of CSD trajectory. For CSDs, the percentage of pixels from each hemisphere recruited into the event was calculated. Of note, clinical seizure duration in human ECT does not consistently include the 0.5-8 second stimulation period, because EEG activity cannot be measured during electrical pulse delivery. Our mouse optical neuroimaging paradigm allows us to observe that high amplitude cortical discharges occur during stimulus delivery; we thus included this activity as part of the seizure.

Both seizure and CSD are well known to trigger a period of suppressed brain activity. To calculate post-event suppression time, a short time Fourier transform (STFT) power spectrum was determined for each pixel and for average right/left hemisphere fluorescence. Hemispheric suppression endpoints were detected using the findchangepts function for the fluorescence signal in each hemisphere. The suppression end point for each pixel was computed by finding the inflection point of up-trending 1-3Hz power (associated with return of slow waves from anesthesia) that is nearest to the respective global suppression endpoint. Then, the suppression duration was computed by taking the difference between the suppression end time and the event (seizure or SD) end time. Suppression times were then averaged within each hemisphere.

The maximum intensity seizure pixel was identified for all end-titration (i.e., CSD-generating) seizures (n=42) by identifying the median value within the top 99% of pixel fluorescence amplitude in seizure maps. We then calculated the shortest distance between the seizure peak pixel and the nearest stimulation electrode (**Fig. 2i**), as well as the shortest distance between the seizure peak pixel and the CSD initiation reference pixel (**Fig. 2j**). Electrode-to-seizure and seizure-to-CSD distances were averaged across all 42 events. To assess the significance of these spatial relationships, a shuffle analysis was conducted by randomly permuting the data and recalculating the average distances for 10,000 iterations. The distribution of shuffled distances was compared to the actual distances, and statistically verified by t-test with Bonferroni correction for multiple comparisons.

253 *Statistical comparisons of seizure and CSD phenotypes*

254 For analyses below summarizing all recorded seizure and CSD events, distribution
255 normality testing was performed using the D'Agostino & Pearson test to determine use of
256 parametric or non-parametric testing. We used non-parametric Kruskal-Wallis ANOVA
257 with Dunn's multiple comparison test for comparison of seizure laterality index between
258 stimulation types (**Fig. 2c**), as well as comparison of seizure duration (Extended Data Fig.
259 3a) and amplitude (**Extended Data Fig. 3a**) across CSD outcomes. Post-event
260 suppression times (**Extended Data Fig. 3c,d**) were compared using the parametric
261 Brown-Forsythe ANOVA with Dunnett's multiple comparison test. The relative
262 contribution of the three types of stimulation configurations (right, left, bilateral) for right,
263 left and bilateral CSDs were compared using Fisher's exact test (**Fig. 2f**). Average CSD
264 fluorescence amplitude (**Fig. 2g**) and duration (**Fig. 2h**) were compared using the non-
265 parametric Mann-Whitney test.

266

267 *Mixed effects model of stimulation parameter titration*

268 For analyses of the effect of titrating pulse parameters (frequency, current level) on
269 seizure properties (overall duration, average mean fluorescence amplitude, **Fig. 3**), we
270 excluded cases that did not cross the seizure threshold in any pixels, thus excluding all
271 evoked responses at 1 mA. A mixed effects model was fit using the outcome of either
272 seizure duration or average peak fluorescence amplitude (%dF/F), transformed on a log
273 scale to achieve approximate normality. Frequency and current level were the
274 independent variables. A model including an interaction between current level and
275 frequency was fit and the interaction evaluated using an F-test with a Satterthwaite

correction for the degrees of freedom. If the interaction was significant ($p < 0.05$) the model was refit for each current level and the effect of increasing frequency evaluated. Specific values of frequency were replaced with integer values (levels 1,2,3,4,5 correspond to 5, 10, 25, 50, 100 Hz) to succinctly evaluate trends in the outcome as a function of frequency. If the interaction was not significant, the procedure was repeated and the main effects of frequency and amplitude were evaluated marginally, followed by Wald tests of specific contrasts. Models of current and frequency effects included electrode placement, animal ID, and pulse counts as covariates to adjust for imbalances across conditions. Electrode placement and pulse count were tested in separate sensitivity analyses to preclude convergence problems with the mixed effects models due to the small number of animals. Similarly, frequency was included as an ordered variable in the model with pulse count.

Time-to-event Model of CSD

To assess how modulating pulse parameters impacts the probability of CSD after seizure, we fit a Cox model substituting current level for time and including frequency as the independent variable and stratification by animal ID. Current is a surrogate for time in this model because an animal receives increasing current levels at each frequency until the event, CSD, is observed. Once a CSD was observed, no further increases in current were assessed. Frequency was considered both as an ordered variable, to assess the overall trend with increasing frequency, and as a categorical variable to describe the results at specific frequencies. Electrode placement is included in the models reported here and in sensitivity analyses substituting pulse count for electrode frequency. Hypothesis tests of

variables with individual terms are based on Wald tests, and for those with multiple categories (electrode placement, frequency) on likelihood ratio tests (LRT). Hypothesis tests are two-sided with a Type I error rate of 0.05, uncorrected for multiple comparisons.

Diffuse Optics and Vitals Monitoring in ECT Patients

All procedures described below were approved by the University of Pennsylvania Institutional Review Board for the observational cohort study, SWEET COMBO: Studying Waves Evoked by Electroconvulsive Therapy with Combined Optical Monitoring of Blood flow and Oxygenation. Patients included in the study (n=18) were recruited from the pool of patients already being treated with ECT at Pennsylvania Hospital (Penn Medicine Health System) between February and July 2024. All participants provided written informed consent to participate. Of note, participation in this cross-sectional study had no impact on which patients were treated with ECT, nor in what manner. All patients were treated with standard of care protocols for Pennsylvania Hospital using a Σigma device (SigmaStim).

During ECT treatment, in addition to routine clinical monitoring (EKG, EEG, vitals), two diffuse optical monitoring probes were placed on the forehead surface in the regions overlying right (F4) and left (F3) prefrontal cortex. The probes and optical system provide simultaneous measurement of blood flow index using diffuse correlation spectroscopy[33,34] (DCS) and tissue oxygen saturation using frequency-domain diffuse optical spectroscopy[34,35] (FD-DOS) from scalp, skull, and cortex underlying the probes (see **Supplemental Methods** on instrumentation)[34]. To improve accuracy of the recovered

322 tissue oxygen saturation, FD-DOS combined data from four separations (1.5, 2, 2.5, and
323 3 cm) on the tissue surface to extract a single datapoint. For DCS flow monitoring, each
324 optical probe utilized a long and short source-detector pair that were fit independently.
325 The light from the short separation pair (1 cm) penetrates scalp and skull, while light from
326 the long separation pair (2.5 cm) probes deeper to the cortex. The optical property data
327 collected concurrently with FD-DOS was input to the DCS fitting to account for changes
328 in absorption and scattering that may otherwise confound the recovered blood flow index.
329 Briefly, FD-DOS and DCS data were fit using the semi-infinite, homogenous solutions to
330 the frequency domain-photon diffusion equation and the correlation diffusion equation,
331 respectively. The interested reader is directed to reference[34] for greater detail on the
332 theoretical models used. In the main text, we only show blood flow obtained from the long
333 separation pair that is sensitive to cortex (example short separation data is shown in
334 **Extended Data Fig. 5** and **Supplemental Discussion**).
335
336 Diffuse optical recordings started from a pre-stimulation baseline period and lasted for
337 several minutes after treatment; the treatment period had variable duration depending on
338 the procedure room schedule, effects of anesthesia, and patient response. Routine
339 intermittent vitals monitoring (collected at 2-minute intervals) was supplemented with
340 continuous vitals monitoring (20 second intervals) using a noninvasive finger monitor for
341 cardiac output (Acumen IQ cuff; HemoSphere monitor, Edwards)[36]. A total of n=27
342 recordings were performed on n=17 patients **(Extended Data Table 2**). Fifteen of these
343 recordings were excluded because the recording signal did not meet quality control
344 standards (see **Supplemental Discussion/Methods**). The remaining n=12 recordings

are presented in **Fig. 4** and **Extended Data Fig. 4**. Secondary post-ictal waves of at least 2-minute duration, and with peak >200% of baseline blood flow and/or with >5% increase above baseline brain oxygen saturation were interpreted as post-ictal CSDs.

Results

ECT seizure is followed by cortical spreading depolarization in mice

We created a new mouse ECT model to facilitate optical neuroimaging of large-scale brain activity during ECT stimulation. We used transgenic *Thy1-jRGECO1a* mice which express the red fluorescent calcium sensor jRGECO1a in excitatory neurons[37]. Mice were implanted with a transparent polymer window overlying the intact skull to enable optical access to activity-dependent dynamics across the cortical surface. We measured neuronal activity with jRGECO1a fluorescence as well as hemodynamic activity with optical intrinsic signal (OIS) imaging, using green light illumination and a 1-photon widefield fluorescence mesoscope (optical set-up shown in **Fig. 1b,** spectra shown in **Extended Data Fig. 1**). To facilitate concurrent electrical stimulation within the imaging field, each mouse cranial window was implanted with five brass electrodes stereotactically affixed to the skull surface overlying frontal, temporo-parietal, and occipital cortices (**Fig. 1a**). Brain activity was recorded with widefield imaging under dexmedetomidine anesthesia during 153 ECT stimulation blocks. To broadly survey the stimulation parameter space (see Methods and **Extended Data Table 1**), we controlled the stimulation pulse parameters using an isolated pulse stimulator, with spatial configuration varied by changing which pair of electrodes were stimulated. For each set of tested

conditions, stimulation was titrated by delivering successive rounds of pulses with increasing current (1, 2, 5, 10, 25 mA, **Fig. 1c**) followed by a monitoring period before restimulating.

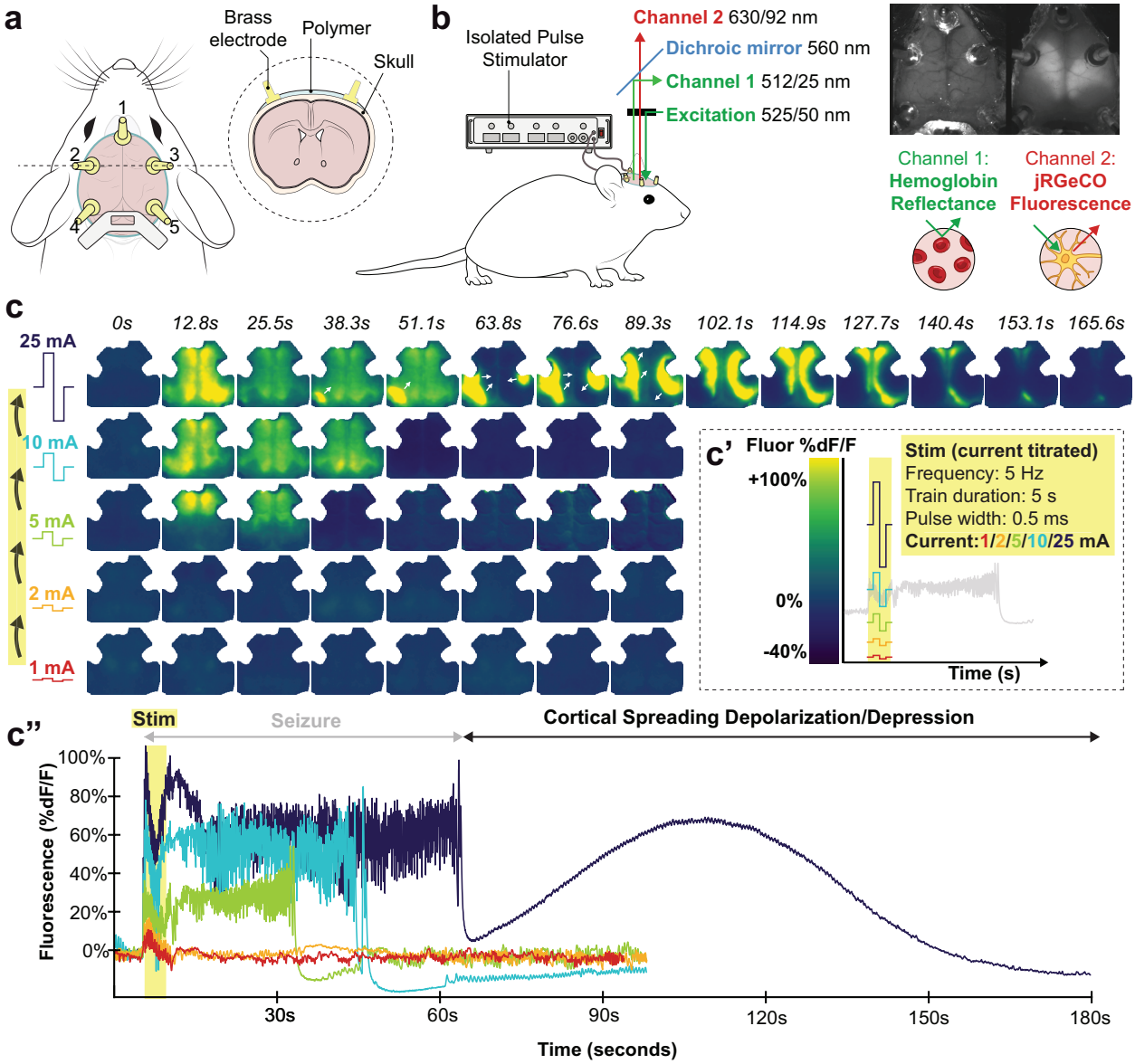

Fig. 1. Optical neuroimaging in a mouse model of ECT demonstrates a current threshold where seizure is followed by cortical spreading depolarization.
a, Schematic of mouse cranial window with optical access to the dorsal cortex. Within each window, five brass electrodes were attached to the intact skull overlying frontal (#1), temporo-parietal (#2, 3), and occipital (#4, 5) cortices.
b, Green-filtered illumination (525/50 nm) was projected through the microscope objective onto the brain; reflected and emitted light from the brain was separated by a 560 nm dichroic mirror into two spatially co-registered channels that were bandpass filtered for isosbestic point hemoglobin reflectance of green illumination (512/25 nm) or jRGECO1a red fluorescence

emission (630/92 nm). Electrical stimulation was delivered via pairs of brass electrode pins using an isolated pulse stimulator. See **Extended Data Fig. 1** and **Supplemental Methods**.
c, Example video frames (from **Extended Data Video 1**) of neuronal activity (jRGECO1a relative fluorescence %dF/F) in an individual mouse being stimulated with 5 Hz pulses to electrodes 1 and 4. Stimulation was titrated in successive rounds with increasing current (**c'**, note rainbow color map corresponds to current titration); in each round we monitored brain activity for 5 seconds of baseline, during stimulation, and then for 90 seconds (or the resumption of baseline slow wave dynamics.). Data from each round of stimulation in the current titration are depicted in still-frame maps of cortical activity in (**c**) and time series averaged within a right hemisphere ROI (**c"**).

Representative neuronal calcium dynamics during ECT titration are shown in **Fig. 1**. Low amplitude current steps (1 and 2 mA) elicited a small <15% dF/F evoked response and then an immediate return of slow wave activity characteristic of anesthesia (**Fig. 1c**). At higher current (5, 10 mA), ECT elicited seizure activity (high amplitude, irregular discharges generalized across the cortex), followed by 5-10 seconds of post-ictal suppression, and then return of slow wave activity. At 25 mA, seizure was followed by a qualitatively distinct electrical event: cortical spreading depolarization (CSD, see **Extended Data Video 1**, depicted as still frames in **Fig. 1c** and time series in **Fig. 1c"**). CSD is a slow-traveling, high amplitude wave of electrochemical depolarization that can be detected with high spatiotemporal fidelity using all-optical detection of neural dynamics or hemodynamics[28-31]. Post-ictal CSD was observed as a slowly propagating, high amplitude wavefront of neuronal calcium elevation that concentrically expanded across the whole brain over the course of ~160 seconds, followed by a prolonged period of suppressed neuronal calcium dynamics. All 38/38 ECT titration sessions reached the threshold to trigger post-ictal CSD. Direct current electrocorticography (DC-ECoG) in a different rodent ECT model likewise demonstrates post-ictal CSD in a current-thresholded manner (see **Extended Data Fig. 2, Supplemental Discussion**).

409 Note, despite their magnitude, CSDs are virtually invisible on routine alternating current
410 (AC)-amplified EEG, as they are physically obscured by volume conduction and spatial
411 blurring through the scalp and skull, and are digitally hidden with high-pass filtering (>0.5
412 Hz)[32,38,39]. Notably, subjecting mouse brain fluorescence data to the same >0.5 Hz high-
413 pass filtering rendered CSD waves invisible on widefield imaging, and at point
414 measurements throughout the brain appeared as a flat line that is otherwise
415 indistinguishable from post-ictal suppression (see **Extended Data Video 1**).
416
417 ***Electrode configuration shapes the spatial topography of seizure and CSD***
418 We then considered whether systematically varying electrode configuration would impact
419 the spatial topography of both seizure and post-ictal CSD waves. In our mouse model
420 with five electrodes, ten electrode pairs were possible for left unilateral (L, green), right
421 unilateral (R, magenta), or bilateral (BL, black) stimulation. Intuitively, we observed that
422 electrode configuration shaped the spatial topography of both the evoked seizure (**Fig.**
423 **2a**, mapping seizure fluorescence amplitude at each pixel) as well as the trajectory of the
424 subsequent CSD traveling wave (**Fig. 2b**, mapping time-to-peak of CSD at each pixel).
425 Bilateral electrode placement produced relatively symmetric seizures, while R or L
426 unilateral electrode placement recruited asymmetric seizure with higher amplitude in the
427 stimulated hemisphere than the contralateral hemisphere (**Fig. 2c,d,** L vs R p****
428 <0.0001, L vs BL p**** <0.0001, R vs BL p** =0.0026).
429

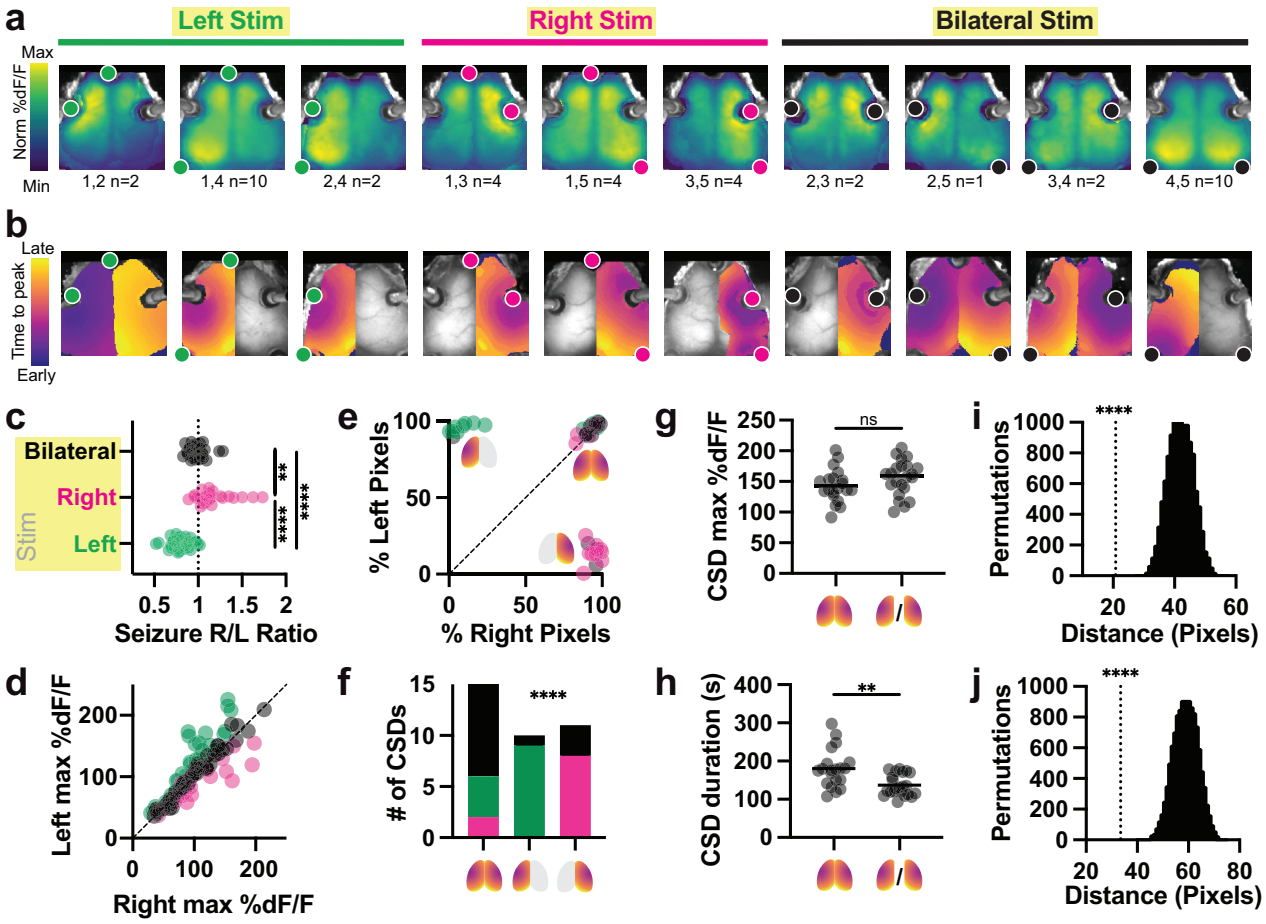

Fig. 2. Electrode configuration shapes the spatial topography of seizure and CSD.
a, Group average maps of seizure amplitude at each pixel (%dF/F). Each panel represents one of 10 possible pairs of 5 electrodes, averaged across multiple stimulation trials (electrode pair and number of trials in each average below, from n=42 end-titration seizures in n=10 mice). Fluorescence colormap is normalized to each plot's min and max; absolute values of fluorescence are shown in **c** and **d**. Stimulated electrode pairs are depicted as colored dots. Note seizures tended to localize near stimulation electrodes.
b, Example individual map of post-ictal CSD trajectory for each electrode configuration, depicting time-to-CSD-peak at each pixel. Note that some CSDs were recruited bilaterally to the entirety of both hemispheres, while others were recruited unilaterally to one hemisphere. Bilateral CSDs typically had some degree of temporal lag between the two hemispheres. Colormaps are normalized to the earliest and latest pixel, with absolute values of overall event durations shown in h.
c, Asymmetry index for all detected seizures across all titrations (see Methods) evoked by right (R, n=25), left (L, n=34) and bilateral (BL, n=38) electrode configurations. Asymmetry index was calculated as the ratio of the left:right hemisphere maximum seizure amplitude averaged across pixels within each hemisphere. Kruskal-Wallis test with Dunn's multiple comparison correction L vs. R (p**** <0.0001), L vs BL (p****<0.0001), R vs BL (p**=0.0026); Kruskal-Wallis statistic 61.83.
d, Seizure amplitude (fluorescence, (%dF/F) values averaged within the right (x-axis) and left (y-axis) hemispheres for each event. A range of frequency and current conditions were tested (see

Fig. 3), producing a wide range of fluorescence intensities. Electrode configuration for each seizure is color coded (L green, R magenta, BL Black).

e, Percentage of pixels within the left hemisphere and right hemisphere where CSD was detected, from n=42 recorded events. Icons depict right-sided, left-sided, and bilateral CSD event types.

f, Distribution of n=39 CSD outcomes resulting from right (magenta), left (green) or bilateral (black) stimulation. Fisher's exact test with null hypothesis that the distributions of electrode configurations are equal in all three CSD outcomes ($p < 0.0001$ for 3x3 interaction).

g, Average amplitude (%dF/F) for bilateral and unilateral CSDs (selecting whichever hemisphere had the largest activation). CSD amplitude was similar whether it occurred in one hemisphere or both, via two-tailed Mann-Whitney test, $p=0.3306$ ($U=171$, $n=42$).

h, Overall duration of bilateral CSDs was slightly longer than that of unilateral CSDs, two-tailed Mann-Whitney test $p^{**}=0.0011$ ($U= 94$, $n=42$). This was due to asymmetry in the start times for each hemisphere, illustrated in bilateral CSDs shown in b.

i, Average distance (pixels) of seizure peak pixel to nearest stimulation electrode (n=42 end-titration seizures), compared to 10,000 permutations of shuffled data, using a two-tailed t-test with Bonferroni corrected $p^{****}<0.0001$.

j, Average distance (pixels) of seizure peak pixel to CSD initiation pixel. Same statistical approach as i.

In contrast to preceding seizures, post-ictal CSDs occurred in an all-or-none fashion anatomically, recruiting either ~0% or ~100% of cortical pixels in a given hemisphere (**Fig. 2b,e**). Trials that evoked bilateral CSD waves were disproportionately triggered by bilateral stimulation, while trials that evoked unilateral CSD waves were disproportionately triggered by same-side unilateral electrodes (**Fig. 2f**, $p <0.0001$). Bilateral and unilateral CSDs tended to achieve similar fluorescence amplitude (**Fig. 2g,** $p= 0.331$), but bilateral CSD events tended to be longer in duration (**Fig. 2h,** $p = 0.0011$), primarily because of cases of asynchronous onset of multi-focal CSD between hemispheres (e.g., **Fig. 2b** frontotemporal configuration 1,2 in panel 1, where CSD in L hemisphere peaked ~1 minute before the R hemisphere). CSD propagation was noted to originate variably from both singleton and multiple foci, with all foci inevitably expanding to invade the entire hemisphere in which they started, but never traveling across midline. Seizure, while always generalized bilaterally throughout cortex, tended to exhibit highest amplitude at a short distance from the stimulation electrodes (**Fig. 2a,i,** $p^{****} <0.0001$), consistent with

484 prior predictions from brain electric field models for various stimulation geometries[5].
485 Likewise, CSD initial foci tended to occur in close spatial proximity to pixels exhibiting
486 peak fluorescence values during the preceding seizure (**Fig. 2b,j**, p**** < 0.0001).
487
488 ***Pulse parameters modulate seizure and post-ictal CSD***
489 Next, we examined titration data to test how pulse parameters, current (mA) and
490 frequency (Hz), influence seizure and CSD. For each treatment session, individual mice
491 were assigned to a pulse frequency and spatial configuration, and then serially stimulated
492 with increasing current steps, monitoring the evoked seizures at each step with optical
493 imaging, and ending at the current threshold where seizure led to CSD. For each seizure,
494 we measured the maximum amplitude (peak fluorescence intensity averaged across all
495 brain pixels, **Fig. 3a**) and overall event duration across the brain (**Fig. 3b**). Current
496 titrations in individual mice at a fixed frequency and electrode configuration are
497 represented as individual lines in **Fig. 3a,b**, with titration curves ending at the current
498 threshold where the evoked seizure triggered a CSD. Some combinations of frequency
499 and current were not tested (e.g., the combination of 100 Hz stimulation at 25 mA was
500 not reached in any titration because all mice experienced CSD at lower current steps).
501 Trials that did not meet our amplitude threshold for defining a seizure (see Methods) were
502 excluded from statistical analysis. To assess how pulse current and frequency modify
503 brain outcomes, we fit a mixed effects model (see Methods), using a random term to
504 account for repeated measures from each animal and fixed effects for the assigned
505 electrode configuration and pulse count.
506

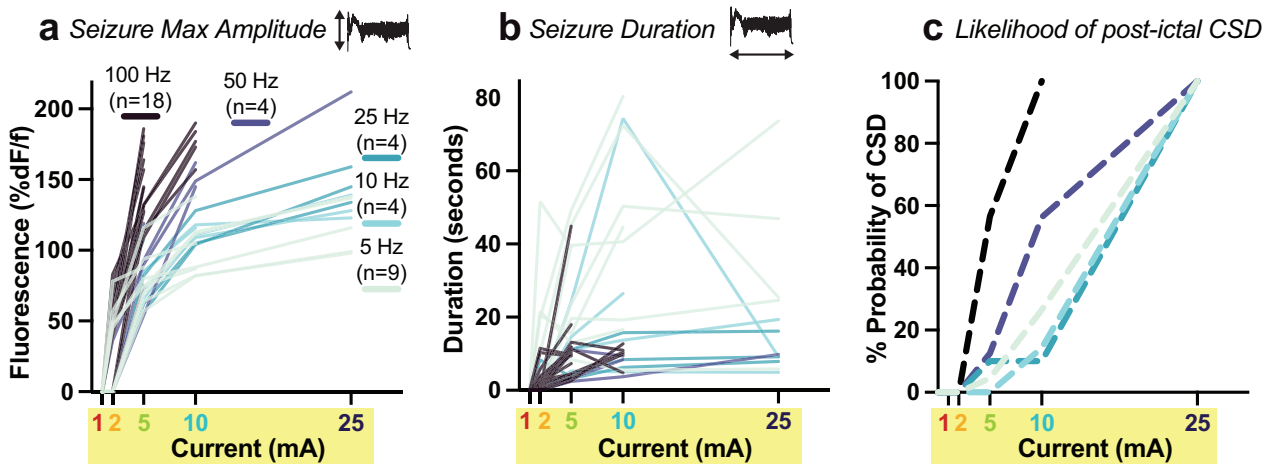

Fig. 3. Pulse current and frequency modulate evoked seizure amplitude and duration, as well as subsequent cortical spreading depolarization. Each mouse was stimulated at fixed pulse frequency (5, 10, 25, 50, or 100 Hz) and then current was increased in a stepwise fashion from 1 mA through 25 mA until a CSD occurred, represented as individual titration lines in **a** and **b**. Titration lines terminate at the CSD threshold current.

a, Seizure amplitude (fluorescence intensity, %dF/F) averaged across the whole cortex as a function of current step within each titration (individual lines). Data analyzed using mixed effects modeling to account for repeated trials on individual animals (see Methods). n is the number of titration trials at a given frequency.

b, Same seizure titrations as in a) but with y-axis measuring seizure duration (seconds), and each line representing the titration of an individual mouse within one of the five frequency groups. Note inversion of the frequency rank order (cool color progression).

c, Cumulative probability of experiencing CSD after seizure at each current step within each frequency condition. See main text for results of statistical analysis.

For every mouse titration, across all tested frequencies, seizure amplitude went up with increasing current (note positive slope to each titration line shown in **Fig. 3a**). The effect of current differed by frequency ($p<0.001$ F-test, with LRT interaction vs. main effects model). Increasing pulse frequency significantly increased the amplitude of the resultant seizure, producing steeper slopes in titrations for higher frequency conditions of 50 and 100 Hz shown in **Fig. 3a**. Within individual current levels, frequency did not significantly modulate seizure amplitude at low current steps (2 mA, $p=0.63$), but each level increase in pulse frequency increased seizure amplitude by a factor of 1.2 fold, significantly so at 5 mA ($p<0.001$) and 10 mA ($p=0.001$), but not at 25 mA ($p=0.11$), see **Fig. 3a**. Electrode placement did not significantly influence seizure amplitude, either in the interaction model

533 (p=0.70) or the individual models (p>0.05). In sensitivity analyses, higher pulse count did
534 not significantly contribute to current and frequency effects (p=0.45 LRT). Higher
535 frequency pulses thus elicit higher amplitude seizures independent of other variables.
536
537 In the same seizure titrations, increasing current led to increased seizure duration (**Fig.**
538 **3b,** p<0.001), in a manner that did not vary significantly by pulse frequency condition
539 (p=0.39). Compared to seizures at the 2 mA current step, seizure duration increased 2.8-
540 fold at 5 mA (p<0.001), 3.5-fold at 10 mA (p<0.001) and 2.8-fold at 25 mA (p=0.005) when
541 controlling for individual frequency level and electrode placement. Somewhat surprisingly,
542 though increasing frequency led to larger seizure amplitude, seizures became briefer.
543 Compared to 5 Hz stimulation, seizure duration decreased by a factor of 0.6 for 10 Hz
544 (p=0.08), by 0.4 at 10 Hz (p=0.004), and by a factor of 0.3 at 50 and 100 Hz (p<0.001).
545 Seizures generally increased in duration with increasing current, but seizures at CSD
546 threshold often had reduced duration, apparently because the expanding CSD terminated
547 the ictal state. Frequency (p<0.001) and pulse count (p=0.006) were associated with
548 longer seizure duration. Delivery of 50 pulses yielded 1.9-fold longer seizure duration
549 than 25 pulses (p=0.006) and 100 pulses yielded 2.4 fold longer seizure duration than
550 25 pulses (p=0.012). Duration at pulse counts of 50 and 100 did not differ significantly
551 from each other. (p=0.49)
552
553 These parameters also impact the probability of generating CSD. Seizures that were
554 sufficient to elicit CSD had significantly higher seizure amplitudes **(Extended Data Fig.**
555 **3**, p < 0.0001 for both unilateral and bilateral CSD), but no difference in seizure duration

556 compared to seizures that do not elicit CSD. We thus asked if higher frequency stimulation
557 (which elicits higher amplitude seizures) was more like to result in a CSD. To this end, we
558 built a Cox model with current level as an analog of time (sequentially increased from 1,
559 2, 5, 10, 25 mA until CSD is achieved) and adjusting for electrode placement and pulse
560 count. We find that increasing the stimulation frequency by one level (e.g., 5 to 10 Hz)
561 increased the cumulative probability of CSD 2.1-fold at any point in the titration (95% CI
562 1.6-2.7, $p<0.001$, **Fig. 3c**). Neither electrode placement ($p=0.199$) nor pulse count
563 ($p=0.64$) was associated with the probability of CSD in this model. Compared to the lowest
564 intensity 5 Hz stimulation, the probability of CSD was 16.5-fold greater at 100 Hz (p
565 <0.001) and 3.5-fold greater, but not significantly so, at 50 Hz ($p=0.23$); 10 Hz ($p=0.83$)
566 and 25 Hz ($p=0.18$) did not differ from 5 Hz. Thus, at any current level, higher stimulation
567 frequency statistically increased the likelihood of eliciting CSD, effectively leading CSD to
568 occur earlier in a titration at lower current. Lastly, we quantified post-event suppression
569 time by measuring the time between the terminal event (seizure or CSD) and subsequent
570 return of baseline slow wave 1-3 Hz spectral power from anesthesia (**Extended Data Fig.**
571 **3c,d**). We observed that post-ictal suppression times were relatively brief (20-70 seconds
572 before return of slow waves), but suppression times were significantly longer in
573 hemispheres affected by CSD (110-270s; see Figure for pairwise comparisons.)
574
575 Using concurrent hemodynamic imaging, we observed that seizure elicited a blush of
576 hyperemia. During CSD, this blush was followed by secondary traveling waves of hypo-
577 and hyperperfusion, which propagated slowly in the wake of the neuronal depolarization
578 wave, consistent with prior reports[30,40]. Intuitively, we observe that bilateral CSD

consistently triggers bilateral hemodynamic traveling waves (**Extended Data Video 2**), unilateral CSD triggers hemodynamic waves in only one hemisphere (**Extended Data Video 3**), and seizure without CSD generates the initial blush, but no post-ictal traveling hemodynamic wave (**Extended Data Video 4**). In each of these videos, two ROI pixel time series are presented to illustrate that CSD hemodynamic waves can occur with a variable post-ictal time delay and morphology, depending on where in the brain one takes a point measurement in the path of a multifocal traveling wave. Optical detection of this hemodynamic wave is a reliable biomarker of CSD in both rodents and humans[28,40-44].

Cerebral hemodynamics in human ECT patients show expected features of post-ictal CSD

Given that CSDs were reliably induced in mice across a wide range of stimulation parameters, we hypothesized that CSDs could also occur in human patients receiving ECT. We further hypothesized that the hemodynamic waves of post-ictal CSD could be translationally detected using non-invasive diffuse optical monitoring of cerebral blood flow and oxygen saturation (**Fig. 4a)**. To this end, we measured local cerebral hemodynamics using multimodal optical sensors on the forehead during routine human ECT treatments in a single-center observational cohort study. Based on our observation of post-ictal CSD waves in mice, we make several predictions. First, we predict that during the EEG post-ictal suppression period, diffuse optical monitoring of cerebral blood flow and oxygen saturation will exhibit a high amplitude, minutes-long hemodynamic surge, with variable wave morphology and time delay relative to the preceding seizure, consistent with prior reports on post-ictal CSD[45]. Second, we predict that this post-ictal

hemodynamic wave will be dissociable from the initial ictal hyperemic blush, and that after seizures that do not elicit CSD, cerebral blood flow and oxygen saturation will return to baseline (similar to **Extended Data Video 4**). Finally, given the impact of electrode spatial configuration on the hemispheric laterality of mouse CSDs (**Fig. 2**), we predict that right unilateral ECT will elicit post-ictal hemodynamic waves that are primarily right sided (and occasionally bilateral), while bilateral stimulation will elicit primarily bilateral CSD waves.

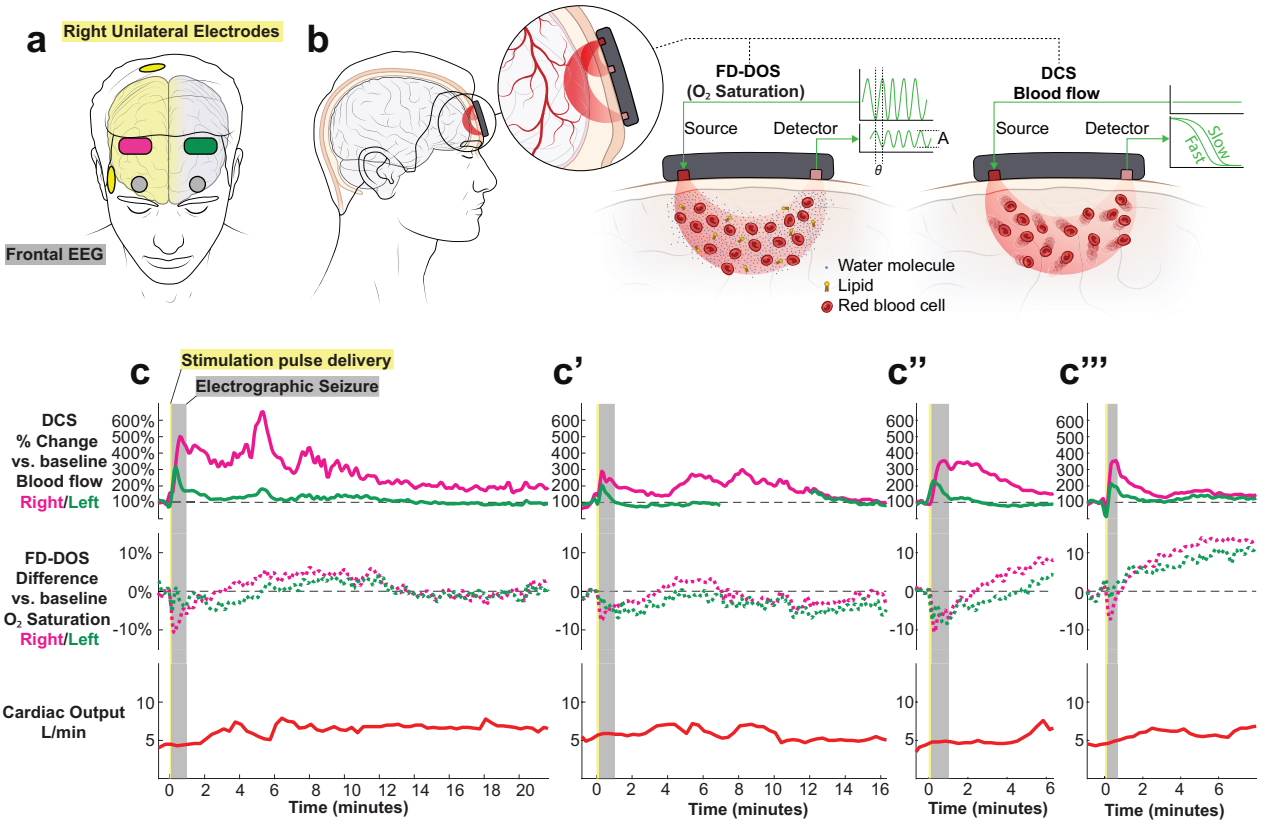

Fig. 4. Cerebral hemodynamics during four ECT sessions from a single patient exhibit expected features of post-ictal CSD.

a, Diagram of diffuse optical probes (magenta on right at F4, green on left at F3), frontal EEG (grey circles at FP1 and FP2), and right unilateral electrodes (yellow).

b, Simplified schematic of non-invasive diffuse optics sensors, using paired red-light sources and detectors to regionally measure both deep (brain) and superficial (skin, scalp) blood flow (diffuse correlation spectroscopy, DCS) from two source-detector separations of 1 cm and 2.5 cm and oxygen saturation (frequency-domain diffuse optical spectroscopy, FD-DOS) from four source-detector separations of 1.5, 2, 2.5, and 3 cm. For clarity, the co-located DCS and FD-DOS probes are separated in the schematic. See **Methods** and **Supplemental Discussion and Methods** on diffuse optics.

c, Series of four recordings on four different treatment days from the same subject receiving right unilateral ECT. Note, the blood flow data shown are derived from the source-detector pair with

largest separation and thus largest depth penetration into the brain (Data at shorter separations are given in **Extended Data Fig. 5**). The oxygen saturation data is the result of combining data from all FD-DOS source-detector pairs for improved signal quality.

In this pilot study, we obtained n=12 recordings of bilateral cerebral hemodynamics during right unilateral ECT (n=5 patients) and bitemporal ECT (n=5 patients), summarized in **Extended Data Table 2**. We first present recordings from four treatments on different days from an index course of right unilateral ECT for a 50-year-old woman with treatment-resistant depression (**Fig. 4b)**. All four treatments resulted in ~60s, bilateral seizures on frontal EEG (grey shaded region). During seizure, relative cerebral blood flow (measured with DCS long source-detector separation) increased by 200-500%. This change was observed predominantly in the right hemisphere, with an associated 5-10% *decrease* in brain %O_2 saturation (derived from the FD-DOS signal).

After the seizure ended electrographically (i.e., scored by a clinician as a flat line on EEG), all four recordings exhibited an inflection point and then a distinct post-ictal wave of 200-600% increase in relative blood flow that lasted several minutes. Interestingly, unlike the preceding seizure, this second hyperemic wave was associated with a 5-10% *increase* in brain oxygen saturation, suggesting that the surge of blood flow kept pace with the metabolic demand of the brain[41,45]. These regional measurements of post-ictal hemodynamic waves exhibited variable waveform morphology and time delay relative to the initial electrographic seizure. In the first three recordings, post-ictal hyperemic waves were restricted to the right hemisphere (magenta lines), and in the last recording the hemodynamic changes occurred bilaterally, indicating three right hemispheric post-ictal events and one bilateral event. These hemispheric comparisons provide a within-subject

control to demonstrate that hemodynamic changes are due to local brain metabolism and not to global autonomic changes. To further corroborate that these 200-600% changes in blood flow index are not due to systemic circulation, we implemented non-invasive cardiac output monitoring throughout the procedure. We observe that systemic blood outflow from the heart was relatively constant at 5 ± 2 L/min throughout the procedure. Taken together, these high-amplitude, minutes-long post-ictal waves of cerebral hyper-perfusion with *increased* oxygen saturation and electrode-configuration-dependent hemispheric laterality, are highly consistent with post-ictal CSD. Of note, over this interval, the patient exhibited a relatively typical clinical response to ECT. At her pre-treatment evaluation she reported intermittent suicidal ideation, anhedonia, excess sleep, feelings of worthlessness, hopelessness, and low energy. After 2 weeks (6 treatments) of ECT, she reported her mood, energy, and sleep had improved, and that her suicidal thoughts had resolved. She denied any side effects of treatment.

We collected eight more recordings from n=8 patients (**Extended Data Fig. 4**) and similarly observed post-ictal hyperemic waves consistent with CSD in an additional 3/3 recordings of right unilateral ECT as well as 4/5 recordings of bitemporal ECT. In all recordings where sensor data was available bilaterally, putative CSDs occurred bilaterally. This post-ictal surge in cerebral blood flow was also evident in the superficial short separation DCS detectors, with variable amplitude relative to the long separation DCS detectors **(**see **Extended Data Fig. 5** and **Supplemental Discussion**). Finally, we provide additional replication cases obtained independently at another institution using a commercial continuous wave functional near infrared spectroscopy (fNIRS) instrument to

670 measure cerebral oximetry in human ECT patients (see **Extended Data Fig. 6** and
671 **Supplemental Discussion**). Thus, the hemodynamic signatures of post-ictal CSD were
672 reliably observed in three different modalities of non-invasive optical monitoring.
673
674
675 **Discussion**
676 In this study, we show that electroconvulsive therapy (ECT) reliably elicits post-ictal
677 cortical spreading depolarization (CSD) in both mouse models and in human patients.
678 This discovery unifies several previously disconnected observations: (1) that ECT induces
679 lasting inhibitory plasticity in brain activity[7], (2) that therapeutic response to ECT requires
680 high energy seizures of sufficient magnitude[46], and (3) that stimulation parameters
681 modulate seizure and clinical outcomes from ECT[20]. Our findings suggest that strong
682 stimulation elicits seizure of sufficient magnitude to generate post-ictal CSD.
683
684 Spreading depolarization may engage mechanisms of inhibitory plasticity that contribute
685 to the brain's clinical response to ECT. Post-ictal CSD is understudied and has primarily
686 been observed in patients with neurologic lesions (e.g., stroke and traumatic brain injury)
687 who have undergone skull-penetrating neurosurgery, thus enabling access for
688 intracranial electrocorticography (ECoG) probes typically used to detect CSD[47-49]. In the
689 context of injury and metabolically fragile brain tissue, CSD is known to exacerbate
690 excitotoxicity and worsen clinical outcomes. However, in the context of seizure in an
691 uninjured brain, preclinical evidence suggests that CSD may act as an intrinsic protective
692 mechanism, terminating the seizure and inducing inhibitory plasticity that prevents future

693 seizures[50,51]. In a healthy brain, CSDs do not cause injury; rather, they induce growth and
694 plasticity genes, downregulate cell death genes, and protect against injury[49,52-55]. Future
695 studies will explore whether CSDs directly contribute to the therapeutic benefit (or side
696 effects) of ECT. One potential clue is the observation that post-ictal blood flow waves
697 were associated with a 5-10% *increase* in cerebral O_2 saturation – a feature associated
698 with CSDs with preserved neurovascular coupling and adequate perfusion, in contrast to
699 the *decreased* O_2 saturation seen in CSDs from ischemic injuries[41]. If CSD proves to be
700 part of the therapeutic mechanism of ECT, this would invite the exciting possibility of
701 bypassing seizure to directly trigger CSD. Indeed, we find that certain stimulation
702 conditions (i.e., brief trains of high frequency pulses) more efficiently generate CSD with
703 minimal seizure duration, while low frequency pulses require higher levels of current to
704 elicit high amplitude seizure or CSD.
705
706 The inhibitory, antiseizure effects of CSD might help explain the long-known inhibitory
707 effects of ECT. ECT raises the seizure threshold in over 90% of patients[7], requiring
708 clinicians to progressively increase stimulation intensity between treatments to maintain
709 adequate seizure[11]. Ironically, this inhibitory effect makes ECT highly effective at treating
710 status epilepticus, particularly in super-refractory cases when maximal anti-seizure
711 pharmacotherapy has failed[56-58]. Furthermore, in those treated with ECT, EEG
712 demonstrates sustained increases in aperiodic power spectral density (an index of cortical
713 inhibitory tone)[59,60], as well as suppressed evoked measures of excitability (transcranial
714 magnetic stimulation evoked potentials)[10]. Human PET imaging has likewise shown that
715 ECT increases cortical GABA concentrations[61], and rodent studies have demonstrated

716 corresponding changes in GABA release[62] and GABA receptor mRNA levels[63]. In the
717 immediate aftermath of CSD, synaptic activity is potently suppressed, initially by
718 depolarization block of axonal action potentials, then by inhibition of presynaptic
719 neurotransmitter release due to activation of adenosine A1 receptors[64,65]. Adenosine
720 accumulation is also observed with seizures[66] and ECT[67]. Within inhibitory circuits, ECT-
721 induced plasticity may require cell-type specific molecular regulators of circuit
722 excitability[68] and act on excitability of single neurons[69]. We hypothesize that post-ictal
723 CSD may contribute to these multi-scale forms of inhibitory plasticity after ECT.
724
725 To our knowledge, this is the first study to record brain activity during ECT pulse delivery.
726 We used optical recordings to circumvent electrical signal artifacts that confound routine
727 EEG monitoring during stimulation. Previous computational predictions have shown that
728 larger evoked electric fields correlate with improved clinical response[15,70,71], which we
729 speculate may be due to increased probability of a large electric field triggering CSD.
730 Real-time recording of brain activity during ECT may prove valuable for future studies on
731 stimulus parameter optimization, just as it has for transcranial magnetic stimulation
732 (TMS)[72-74], deep brain stimulation (DBS)[75,76], and ultrasound neuromodulation[77]. Of note,
733 in our mouse model, we observed that high frequency stimulation at 100 Hz sometimes
734 evoked only a single high amplitude spike during pulse delivery, without persistent post-
735 stimulation ictal activity. We opted to include evoked activity during stimulation as part of
736 the seizure, though the physiology governing persistent post-stimulation seizure may be
737 different than acute evoked discharges during stimulation. Both brief high amplitude
738 discharges during stimulation as well as persistent post-stimulation seizure were sufficient

739 to generate CSD in our mouse model. We similarly observed post-ictal CSD in mouse
740 electrocorticography recordings, consistent with prior reports[78-80]. In human subjects,
741 electrographic verification of post-ictal CSD during ECT is not feasible due to lack of
742 intracranial access for a non-invasive procedure. Optical monitoring of brain activity has
743 been cross-validated as a surrogate for electrophysiologic CSD detection in mice and
744 humans, providing rich spatial detail on traveling waves[28,40-44].
745
746 Post-ictal CSD has the potential to explain many epiphenomena seen in other
747 measurements of brain activity from ECT patients. We observed that larger seizures were
748 more likely to generate CSD in mice, which could theoretically explain why higher EEG
749 ictal spectral power is associated with improved clinical outcomes in humans[12,14,15]. Our
750 rodent data also showed longer post-event suppression time after CSD compared to
751 seizure alone, which could explain why longer suppression times are associated with
752 improved patient outcomes[12,81] and longer latency to reorientation[82]. Extended EEG
753 recording after treatment may be necessary to validate if post-ictal suppression is
754 associated with CSD[39,83]. Looking beyond EEG, CSD is known to produce lasting
755 changes in brain hemodynamics, which could account for why effective ECT seizures
756 elicit lasting perfusion changes 1-hour after treatment[84] as well as on longer
757 timescales[85,86]. Furthermore, we observed that right unilateral stimulation primarily
758 generated unilateral post-ictal waves. Unilateral CSD could play a role in ECT-induced
759 volumetric changes that occur preferentially in the stimulated hemisphere and correlate
760 with clinical outcomes and brain network functional connectivity changes[87-92]. CSDs are
761 so named because neocortex is most accessible for recording brain activity. Indeed, this

762 is a key limitation of our optical methods for recording cortical dynamics - spreading
763 depolarization can also occur in subcortical structures, which might have important
764 implications for both the clinical benefits and side effects of ECT.
765
766 We speculate that post-ictal CSD has been occurring undetected during the millions of
767 treatments that have been performed over the last 86 years. In clinical practice, EEG is
768 typically turned off after the seizure terminates, and furthermore, EEG cannot reliably
769 detect CSDs [32,38] unless the skull has been penetrated[39,93]. This is thought to be due to
770 digital high-pass filtering of slow waveforms, as well as spatial smearing from volume
771 conduction of CSD dynamics through the brain, skull, and scalp. Very focal CSDs with
772 narrow-width wavefronts may be particularly challenging to detect[39].
773
774 Dreier et al. have proposed that non-invasive optical hemodynamic measures might prove
775 sufficient to detect CSD in human patients[93]. Here we indeed find evidence that optical
776 features of CSD can be detected non-invasively at patient bedside. This approach to CSD
777 detection may have valuable clinical applications in neurocritical care for individuals
778 without intracranial ECoG implants. Previous studies have characterized the
779 hemodynamic features of CSD using invasive probes in the brain[94,95], or non-invasively
780 using functional MRI[96] and PET imaging[97]. In this study we implemented an
781 investigational device that combined frequency-domain diffuse optical spectroscopy (FD-
782 DOS) to measure tissue oxygenation with diffuse correlation spectroscopy (DCS) to
783 capture blood flow rate changes. Our optical probes have several limitations. Our
784 approach relied on regional point measurements over non-hair bearing skin. Future

785 investigations using broader spatial coverage at multiple points would be needed to detect
786 CSD propagation across a brain hemisphere. In addition, signal quality is significantly
787 influenced by patient motion, skin temperature, and variation in skull and skin
788 microanatomy that can influence the detected optical path distribution (see
789 **Supplemental Discussion/Methods**). These factors can introduce systematic errors
790 that influence absolute tissue optical properties. We have ameliorated these effects by
791 computing relative change in blood flow and oxygenation indices within each individual.
792
793 This study implemented a new mouse model of ECT that enabled experimental control
794 over stimulation combined with real-time monitoring of brain activity with widefield
795 imaging. To model the three standard ECT electrode placements (right unilateral,
796 bitemporal, bifrontal), we attached five electrodes to the intact skull with silver-conductive
797 epoxy to test ten configurations of electrode pairs. This builds on prior innovation using
798 screw electrodes in rats, which have been shown to have superior translational validity to
799 conventional rodent ECT with auricular (ear clip) electrodes.[98] Skull electrodes help
800 control for the confounding effects of current shunting through the low-resistance skin[99].
801 Indeed, we observed the use of ear clip electrodes required 5-10 times more current to
802 elicit seizure or CSD compared to skull electrodes (see **Supplement**). In addition, we
803 substituted a conventional rodent ECT device for a broadly customizable isolated pulse
804 stimulator, enabling the first systematic evaluation of ECT pulse parameters in an animal
805 model. We found that increasing pulse frequency increased seizure amplitude and
806 probability of CSD, while low frequency pulses elicited long duration seizures without
807 increased probability of CSD. This builds on prior studies showing that high frequency

electrical pulses can elicit CSD in hippocampal slices[100], and that low intensity stimulation does not elicit CSD[101]. One limitation of this study is its inability to exhaustively survey the virtually infinite space of pulse parameters and electrode configurations[20]. We opted to survey multiple electrode and pulse parameters simultaneously, using pseudorandomization to sample stimulation conditions in a balanced fashion and linear mixed effects modeling to isolate pulse parameter-specific effects in titration data. This is an imperfect solution, and future investigations would benefit from systematically modulating individual stimulation parameters, as well as testing for specific effects in translational models of neuropsychiatric disease. Lastly, using a current titration strategy, we identified that increasing pulse frequency lowered the current threshold required to elicit a seizure of a given magnitude. This has important ramifications for novel ECT protocols that modulate current amplitude[26,71,102]. Future investigations should explore whether high frequency stimulation is a more current-sparing approach of achieving therapeutic efficacy. This study thus provides a translational framework for measuring brain activity to optimize ECT stimulation parameters and precisely control seizure and post-ictal CSD. These findings further highlight opportunities to modernize ECT and directly target treatment-induced mechanisms of brain plasticity.

Author Contributions:
All authors helped with data interpretation and editorial feedback on the paper.
ZPR conceptualized overall project; designed, performed, and analyzed results of mouse experiments; generated Penn IRB protocol, collected and analyzed human data; wrote original manuscript, produced figures; contributed funding.
JBM contributed to diffuse optics method development, human data collection and analysis, and text in the original manuscript
AS contributed to Penn mouse imaging data analysis and text in the original manuscript
DKQ designed and performed UNM human recordings
BEL contributed UNM mouse recordings and text in the original manuscript.
MEP conceptualized and implemented time-to-event and linear mixed effects modeling and contributed text in the original manuscript.
AK contributed to the statistical analysis presented in the original manuscript.
CGF contributed to methodological development of human studies and IRB protocol.
WBB contributed to conceptualization and methods development for diffuse optics.
GH is an ECT clinician who helped supervise human data collection.
JPR is an ECT clinician who helped supervise human data collection.
MAC is an ECT clinician who helped supervise human data collection and advise on project conceptualization.
YIS helped supervise development of human studies and funding acquisition.
CWS conceptualized and supervised UNM mouse experiments.
CCA is an ECT clinician and conceptualized and supervised UNM human case series.
AGY contributed diffuse optics resources for human recordings, method development, data analysis, postdoctoral supervision and funding support of JBM.
EMG contributed to method development of mouse ECT model and widefield imaging, editorial supervision of original manuscript, postdoctoral supervision of ZPR.

Acknowledgements: We would like to thank the patients who participated in the study for their generosity and openness. This work was supported by the Penn Psychiatry Residency Research Track award NIH R25MH119043 (ZPR); Institute for Translational Medicine and Therapeutics of the University of Pennsylvania NIH UL1TR001878 (ZPR); NIH P41-EB029460 (AGY); NIH NS078805, NS051288, NS070680 (BEL); NIH NS106901 (CWS); NIH P50HD105354 (MEP, AK). The authors would like to thank Emily Hoddeson for assistance with mouse husbandry and genotyping, Dr. Adam Bauer for advice on mouse optical methods, ANT Neuro for loaning DC-EEG equipment, Katy Brown for facilitating human continuous vitals monitoring, Dr. Holly Lisanby for advice on project conceptualization, Jurre Blom for assistance with manuscript illustrations, Dr. Brian White for help launching the collaboration between the diffuse optics and ECT research teams, and Dr. Rodrigo M. Forti for help with data interpretation and diffuse optical instrumentation.

Competing Interests: No financial conflicts or completing interests to disclose.

Data Availability Code used in this project will be uploaded to the Goldberg Lab github repository (https://github.com/GoldbergNeuroLab) and data will be uploaded to gnode (https://gin.g-node.org/GoldbergNeuroLab).

References:

1. Espinoza, R. T. & Kellner, C. H. Electroconvulsive Therapy. *N Engl J Med* **386**, 667-672, (2022).
2. Kaster, T. S., Blumberger, D. M., Gomes, T., Sutradhar, R., Wijeysundera, D. N. & Vigod, S. N. Risk of suicide death following electroconvulsive therapy treatment for depression: a propensity score-weighted, retrospective cohort study in Canada. *Lancet Psychiatry* **9**, 435-446, (2022).
3. Fink, M. What was learned: studies by the consortium for research in ECT (CORE) 1997-2011. *Acta Psychiatr Scand* **129**, 417-426, (2014).
4. Sackeim, H. A. Modern Electroconvulsive Therapy: Vastly Improved yet Greatly Underused. *JAMA Psychiatry* **74**, 779-780, (2017).
5. Deng, Z. D., Robins, P. L., Regenold, W., Rohde, P., Dannhauer, M. & Lisanby, S. H. How electroconvulsive therapy works in the treatment of depression: is it the seizure, the electricity, or both? *Neuropsychopharmacology* **49**, 150-162, (2024).
6. Regenold, W. T., Noorani, R. J., Piez, D. & Patel, P. Nonconvulsive Electrotherapy for Treatment Resistant Unipolar and Bipolar Major Depressive Disorder: A Proof-of-concept Trial. *Brain Stimul* **8**, 855-861, (2015).
7. Duthie, A. C., Perrin, J. S., Bennett, D. M., Currie, J. & Reid, I. C. Anticonvulsant Mechanisms of Electroconvulsive Therapy and Relation to Therapeutic Efficacy. *J ECT* **31**, 173-178, (2015).
8. Lloyd, R. L. & Sattin, A. The Behavioral Physiology and Antidepressant Mechanisms of Electroconvulsive Shock. *J ECT* **31**, 159-166, (2015).
9. Voineskos, D., Levinson, A. J., Sun, Y., Barr, M. S., Farzan, F., Rajji, T. K., Fitzgerald, P. B., Blumberger, D. M. & Daskalakis, Z. J. The Relationship Between Cortical Inhibition and Electroconvulsive Therapy in the Treatment of Major Depressive Disorder. *Sci Rep* **6**, 37461, (2016).
10. Bajbouj, M., Lang, U. E., Niehaus, L., Hellen, F. E., Heuser, I. & Neu, P. Effects of right unilateral electroconvulsive therapy on motor cortical excitability in depressive patients. *J Psychiatr Res* **40**, 322-327, (2006).
11. Krystal, A. D., Coffey, C. E., Weiner, R. D. & Holsinger, T. Changes in seizure threshold over the course of electroconvulsive therapy affect therapeutic response and are detected by ictal EEG ratings. *J Neuropsychiatry Clin Neurosci* **10**, 178-186, (1998).
12. Perera, T. D., Luber, B., Nobler, M. S., Prudic, J., Anderson, C. & Sackeim, H. A. Seizure expression during electroconvulsive therapy: relationships with clinical outcome and cognitive side effects. *Neuropsychopharmacology* **29**, 813-825, (2004).
13. Zhang, J. Y., Xu, S. X., Zeng, L., Chen, L. C., Li, J., Jiang, Z. Y., Tan, B. J., Gu, C. L., Lai, W. T., Kong, X. M., Wang, J., Rong, H. & Xie, X. H. Improved Safety of Hybrid Electroconvulsive Therapy Compared With Standard Electroconvulsive Therapy in Patients With Major Depressive Disorder: A Randomized, Double-Blind, Parallel-Group Pilot Trial. *Front Psychiatry* **13**, 896018, (2022).

919 14. Miller, J., Jones, T., Upston, J., Deng, Z. D., McClintock, S. M., Ryman, S., Quinn, D. &
920 Abbott, C. C. Ictal Theta Power as an Electroconvulsive Therapy Safety Biomarker: A
921 Pilot Study. *J ECT* **38**, 88-94, (2022).
922 15. Miller, J., Jones, T., Upston, J., Deng, Z. D., McClintock, S. M., Erhardt, E., Farrar, D. &
923 Abbott, C. C. Electric Field, Ictal Theta Power, and Clinical Outcomes in
924 Electroconvulsive Therapy. *Biol Psychiatry Cogn Neurosci Neuroimaging* **8**, 760-767,
925 (2023).
926 16. Gillving, C., Ekman, C. J., Hammar, A., Landen, M., Lundberg, J., Movahed Rad, P.,
927 Nordanskog, P., von Knorring, L. & Nordenskjold, A. Seizure Duration and
928 Electroconvulsive Therapy in Major Depressive Disorder. *JAMA Netw Open* **7**,
929 e2422738, (2024).
930 17. Khadka, N., Deng, Z. D., Lisanby, S. H., Bikson, M. & Camprodon, J. A. Computational
931 Models of High-Definition Electroconvulsive Therapy for Focal or Multitargeting
932 Treatment. *J ECT*, (2024).
933 18. Argyelan, M. *et al.* Electroconvulsive therapy-induced volumetric brain changes converge on
934 a common causal circuit in depression. *Mol Psychiatry* **29**, 229-237, (2024).
935 19. Deng, Z. D., Argyelan, M., Miller, J., Quinn, D. K., Lloyd, M., Jones, T. R., Upston, J.,
936 Erhardt, E., McClintock, S. M. & Abbott, C. C. Electroconvulsive therapy, electric field,
937 neuroplasticity, and clinical outcomes. *Mol Psychiatry* **27**, 1676-1682, (2022).
938 20. Peterchev, A. V., Rosa, M. A., Deng, Z. D., Prudic, J. & Lisanby, S. H. Electroconvulsive
939 therapy stimulus parameters: rethinking dosage. *J ECT* **26**, 159-174, (2010).
940 21. Sackeim, H. A., Prudic, J., Nobler, M. S., Fitzsimons, L., Lisanby, S. H., Payne, N., Berman,
941 R. M., Brakemeier, E. L., Perera, T. & Devanand, D. P. Effects of pulse width and
942 electrode placement on the efficacy and cognitive effects of electroconvulsive therapy.
943 *Brain Stimul* **1**, 71-83, (2008).
944 22. Wang, X., Padawer-Curry, J. A., Bice, A. R., Kim, B., Rosenthal, Z. P., Lee, J.-M., Goyal,
945 M. S., Macauley, S. L. & Bauer, A. Q. Spatiotemporal relationships between neuronal,
946 metabolic, and hemodynamic signals in the awake and anesthetized mouse brain. *Cell*
947 *Reports* **43**, (2024).
948 23. Brier, L. M., Landsness, E. C., Snyder, A. Z., Wright, P. W., Baxter, G. A., Bauer, A. Q.,
949 Lee, J. M. & Culver, J. P. Separability of calcium slow waves and functional connectivity
950 during wake, sleep, and anesthesia. *Neurophotonics* **6**, 035002, (2019).
951 24. Mitra, A., Kraft, A., Wright, P., Acland, B., Snyder, A. Z., Rosenthal, Z., Czerniewski, L.,
952 Bauer, A., Snyder, L., Culver, J., Lee, J. M. & Raichle, M. E. Spontaneous Infra-slow
953 Brain Activity Has Unique Spatiotemporal Dynamics and Laminar Structure. *Neuron* **98**,
954 297-305 e296, (2018).
955 25. Mukhtar, F., Regenold, W. & Lisanby, S. H. Recent advances in electroconvulsive therapy in
956 clinical practice and research. *Faculty Reviews* **12**, (2023).
957 26. Peterchev, A. V., Krystal, A. D., Rosa, M. A. & Lisanby, S. H. Individualized Low-
958 Amplitude Seizure Therapy: Minimizing Current for Electroconvulsive Therapy and
959 Magnetic Seizure Therapy. *Neuropsychopharmacology* **40**, 2076-2084, (2015).
960 27. Franklin, K. B. J. & Paxinos, G. *The Mouse Brain in Stereotactic Coordinates*. (Academic
961 Press, 2012).
962 28. Chung, D. Y., Sugimoto, K., Fischer, P., Bohm, M., Takizawa, T., Sadeghian, H., Morais, A.,
963 Harriott, A., Oka, F., Qin, T., Henninger, N., Yaseen, M. A., Sakadzic, S. & Ayata, C.

Real-time non-invasive in vivo visible light detection of cortical spreading depolarizations in mice. *J Neurosci Methods* **309**, 143-146, (2018).

29. Balbi, M., Vanni, M. P., Silasi, G., Sekino, Y., Bolanos, L., LeDue, J. M. & Murphy, T. H. Targeted ischemic stroke induction and mesoscopic imaging assessment of blood flow and ischemic depolarization in awake mice. *Neurophotonics* **4**, 035001, (2017).

30. Zhao, H. T., Tuohy, M. C., Chow, D., Kozberg, M. G., Kim, S. H., Shaik, M. A. & Hillman, E. M. C. Neurovascular dynamics of repeated cortical spreading depolarizations after acute brain injury. *Cell Rep* **37**, 109794, (2021).

31. Smith, S. E. *et al.* Astrocyte deletion of alpha2-Na/K ATPase triggers episodic motor paralysis in mice via a metabolic pathway. *Nat Commun* **11**, 6164, (2020).

32. Hofmeijer, J., van Kaam, C. R., van de Werff, B., Vermeer, S. E., Tjepkema-Cloostermans, M. C. & van Putten, M. Detecting Cortical Spreading Depolarization with Full Band Scalp Electroencephalography: An Illusion? *Front Neurol* **9**, 17, (2018).

33. Carp, S. A., Robinson, M. B. & Franceschini, M. A. Diffuse correlation spectroscopy: current status and future outlook. *Neurophotonics* **10**, 013509, (2023).

34. Durduran, T., Choe, R., Baker, W. B. & Yodh, A. G. Diffuse Optics for Tissue Monitoring and Tomography. *Rep Prog Phys* **73**, (2010).

35. Zhou, X., Xia, Y., Uchitel, J., Collins-Jones, L., Yang, S., Loureiro, R., Cooper, R. J. & Zhao, H. Review of recent advances in frequency-domain near-infrared spectroscopy technologies [Invited]. *Biomed Opt Express* **14**, 3234-3258, (2023).

36. Kouz, K. *et al.* Intraoperative hypotension when using hypotension prediction index software during major noncardiac surgery: a European multicentre prospective observational registry (EU HYPROTECT). *BJA Open* **6**, 100140, (2023).

37. Dana, H., Novak, O., Guardado-Montesino, M., Fransen, J. W., Hu, A., Borghuis, B. G., Guo, C., Kim, D. S. & Svoboda, K. Thy1 transgenic mice expressing the red fluorescent calcium indicator jRGECO1a for neuronal population imaging in vivo. *PLoS One* **13**, e0205444, (2018).

38. Dreier, J. P., Major, S., Lemale, C. L., Kola, V., Reiffurth, C., Schoknecht, K., Hecht, N., Hartings, J. A. & Woitzik, J. Correlates of Spreading Depolarization, Spreading Depression, and Negative Ultraslow Potential in Epidural Versus Subdural Electrocorticography. *Front Neurosci* **13**, 373, (2019).

39. Chamanzar, A., George, S., Venkatesh, P., Chamanzar, M., Shutter, L., Elmer, J. & Grover, P. An Algorithm for Automated, Noninvasive Detection of Cortical Spreading Depolarizations Based on EEG Simulations. *IEEE Trans Biomed Eng* **66**, 1115-1126, (2019).

40. Ayata, C., Shin, H. K., Salomone, S., Ozdemir-Gursoy, Y., Boas, D. A., Dunn, A. K. & Moskowitz, M. A. Pronounced hypoperfusion during spreading depression in mouse cortex. *J Cereb Blood Flow Metab* **24**, 1172-1182, (2004).

41. Dreier, J. P. The role of spreading depression, spreading depolarization and spreading ischemia in neurological disease. *Nat Med* **17**, 439-447, (2011).

42. de Crespigny, A., Rother, J., van Bruggen, N., Beaulieu, C. & Moseley, M. E. Magnetic resonance imaging assessment of cerebral hemodynamics during spreading depression in rats. *J Cereb Blood Flow Metab* **18**, 1008-1017, (1998).

43. Zhou, C., Yu, G., Furuya, D., Greenberg, J., Yodh, A. & Durduran, T. Diffuse optical correlation tomography of cerebral blood flow during cortical spreading depression in rat brain. *Opt Express* **14**, 1125-1144, (2006).

1010 44. Yamato, H., Jin, T. & Nomura, Y. Near infrared imaging of intrinsic signals in cortical
1011 spreading depression observed through the intact scalp in hairless mice. *Neurosci Lett*
1012 **701**, 213-217, (2019).
1013 45. Winkler, M. K., Dengler, N., Hecht, N., Hartings, J. A., Kang, E. J., Major, S., Martus, P.,
1014 Vajkoczy, P., Woitzik, J. & Dreier, J. P. Oxygen availability and spreading
1015 depolarizations provide complementary prognostic information in neuromonitoring of
1016 aneurysmal subarachnoid hemorrhage patients. *J Cereb Blood Flow Metab* **37**, 1841-
1017 1856, (2017).
1018 46. Sackeim, H. A., Prudic, J., Devanand, D. P., Kiersky, J. E., Fitzsimons, L., Moody, B. J.,
1019 McElhiney, M. C., Coleman, E. A. & Settembrino, J. M. Effects of stimulus intensity and
1020 electrode placement on the efficacy and cognitive effects of electroconvulsive therapy. *N*
1021 *Engl J Med* **328**, 839-846, (1993).
1022 47. Fabricius, M., Fuhr, S., Willumsen, L., Dreier, J. P., Bhatia, R., Boutelle, M. G., Hartings, J.
1023 A., Bullock, R., Strong, A. J. & Lauritzen, M. Association of seizures with cortical
1024 spreading depression and peri-infarct depolarisations in the acutely injured human brain.
1025 *Clin Neurophysiol* **119**, 1973-1984, (2008).
1026 48. Dreier, J. P., Major, S., Pannek, H. W., Woitzik, J., Scheel, M., Wiesenthal, D., Martus, P.,
1027 Winkler, M. K., Hartings, J. A., Fabricius, M., Speckmann, E. J., Gorji, A. & group, C. s.
1028 Spreading convulsions, spreading depolarization and epileptogenesis in human cerebral
1029 cortex. *Brain* **135**, 259-275, (2012).
1030 49. Dreier, J. P. *et al.* Recording, analysis, and interpretation of spreading depolarizations in
1031 neurointensive care: Review and recommendations of the COSBID research group. *J*
1032 *Cereb Blood Flow Metab* **37**, 1595-1625, (2017).
1033 50. Zakharov, A., Chernova, K., Burkhanova, G., Holmes, G. L. & Khazipov, R. Segregation of
1034 seizures and spreading depolarization across cortical layers. *Epilepsia* **60**, 2386-2397,
1035 (2019).
1036 51. Tamim, I., Chung, D. Y., de Morais, A. L., Loonen, I. C. M., Qin, T., Misra, A., Schlunk, F.,
1037 Endres, M., Schiff, S. J. & Ayata, C. Spreading depression as an innate antiseizure
1038 mechanism. *Nat Commun* **12**, 2206, (2021).
1039 52. Dell'Orco, M., Weisend, J. E., Perrone-Bizzozero, N. I., Carlson, A. P., Morton, R. A.,
1040 Linsenbardt, D. N. & Shuttleworth, C. W. Repetitive spreading depolarization induces
1041 gene expression changes related to synaptic plasticity and neuroprotective pathways.
1042 *Front Cell Neurosci* **17**, 1292661, (2023).
1043 53. Nedergaard, M. & Hansen, A. J. Spreading depression is not associated with neuronal injury
1044 in the normal brain. *Brain Res* **449**, 395-398, (1988).
1045 54. Kobayashi, S., Harris, V. A. & Welsh, F. A. Spreading depression induces tolerance of
1046 cortical neurons to ischemia in rat brain. *J Cereb Blood Flow Metab* **15**, 721-727, (1995).
1047 55. Matsushima, K., Hogan, M. J. & Hakim, A. M. Cortical spreading depression protects
1048 against subsequent focal cerebral ischemia in rats. *J Cereb Blood Flow Metab* **16**, 221-
1049 226, (1996).
1050 56. Lambrecq, V., Villega, F., Marchal, C., Michel, V., Guehl, D., Rotge, J. Y. & Burbaud, P.
1051 Refractory status epilepticus: electroconvulsive therapy as a possible therapeutic strategy.
1052 *Seizure* **21**, 661-664, (2012).
1053 57. Garcia-Lopez, B. *et al.* Electroconvulsive Therapy in Super Refractory Status Epilepticus:
1054 Case Series with a Defined Protocol. *Int J Environ Res Public Health* **17**, (2020).

1055 58. Ahmed, J., Metrick, M., Gilbert, A., Glasson, A., Singh, R., Ambrous, W., Brown, L.,
1056 Aykroyd, L. & Bobel, K. Electroconvulsive Therapy for Super Refractory Status
1057 Epilepticus. *J ECT* **34**, e5-e9, (2018).
1058 59. Smith, S. E., Ma, V., Gonzalez, C., Chapman, A., Printz, D., Voytek, B. & Soltani, M.
1059 Clinical EEG slowing induced by electroconvulsive therapy is better described by
1060 increased frontal aperiodic activity. *Transl Psychiatry* **13**, 348, (2023).
1061 60. Smith, S. E., Kosik, E. L., van Engen, Q., Kohn, J., Hill, A. T., Zomorrodi, R., Blumberger,
1062 D. M., Daskalakis, Z. J., Hadas, I. & Voytek, B. Magnetic seizure therapy and
1063 electroconvulsive therapy increase aperiodic activity. *Transl Psychiatry* **13**, 347, (2023).
1064 61. Sanacora, G., Mason, G. F., Rothman, D. L., Hyder, F., Ciarcia, J. J., Ostroff, R. B., Berman,
1065 R. M. & Krystal, J. H. Increased cortical GABA concentrations in depressed patients
1066 receiving ECT. *Am J Psychiatry* **160**, 577-579, (2003).
1067 62. Green, A. R. & Vincent, N. D. The effect of repeated electroconvulsive shock on GABA
1068 synthesis and release in regions of rat brain. *Br J Pharmacol* **92**, 19-24, (1987).
1069 63. Kang, I., Miller, L. G., Moises, J. & Bazan, N. G. GABAA receptor mRNAs are increased
1070 after electroconvulsive shock. *Psychopharmacol Bull* **27**, 359-363, (1991).
1071 64. Lindquist, B. E. & Shuttleworth, C. W. Adenosine receptor activation is responsible for
1072 prolonged depression of synaptic transmission after spreading depolarization in brain
1073 slices. *Neuroscience* **223**, 365-376, (2012).
1074 65. Lindquist, B. E. & Shuttleworth, C. W. Evidence that adenosine contributes to Leao's
1075 spreading depression in vivo. *J Cereb Blood Flow Metab* **37**, 1656-1669, (2017).
1076 66. Boison, D. Adenosinergic signaling in epilepsy. *Neuropharmacology* **104**, 131-139, (2016).
1077 67. Lewin, E. & Bleck, V. Electroshock seizures in mice: effect on brain adenosine and its
1078 metabolites. *Epilepsia* **22**, 577-581, (1981).
1079 68. Chang, A. D. *et al.* Narp Mediates Antidepressant-Like Effects of Electroconvulsive
1080 Seizures. *Neuropsychopharmacology* **43**, 1088-1098, (2018).
1081 69. Ueta, Y., Yamamoto, R. & Kato, N. Layer-specific modulation of pyramidal cell excitability
1082 by electroconvulsive shock. *Neurosci Lett* **709**, 134383, (2019).
1083 70. Lee, W. H., Lisanby, S. H., Laine, A. F. & Peterchev, A. V. Comparison of electric field
1084 strength and spatial distribution of electroconvulsive therapy and magnetic seizure
1085 therapy in a realistic human head model. *Eur Psychiatry* **36**, 55-64, (2016).
1086 71. Abbott, C. C., Quinn, D., Miller, J., Ye, E., Iqbal, S., Lloyd, M., Jones, T. R., Upston, J.,
1087 Deng, Z., Erhardt, E. & McClintock, S. M. Electroconvulsive Therapy Pulse Amplitude
1088 and Clinical Outcomes. *Am J Geriatr Psychiatry* **29**, 166-178, (2021).
1089 72. Gogulski, J., Ross, J. M., Talbot, A., Cline, C. C., Donati, F. L., Munot, S., Kim, N., Gibbs,
1090 C., Bastin, N., Yang, J., Minasi, C., Sarkar, M., Truong, J. & Keller, C. J. Personalized
1091 Repetitive Transcranial Magnetic Stimulation for Depression. *Biol Psychiatry Cogn*
1092 *Neurosci Neuroimaging* **8**, 351-360, (2023).
1093 73. Wang, J. B., Hassan, U., Bruss, J. E., Oya, H., Uitermarkt, B. D., Trapp, N. T., Gander, P. E.,
1094 Howard, M. A., 3rd, Keller, C. J. & Boes, A. D. Effects of transcranial magnetic
1095 stimulation on the human brain recorded with intracranial electrocorticography. *Mol*
1096 *Psychiatry* **29**, 1228-1240, (2024).
1097 74. Peterchev, A. V., Goetz, S. M., Westin, G. G., Luber, B. & Lisanby, S. H. Pulse width
1098 dependence of motor threshold and input-output curve characterized with controllable
1099 pulse parameter transcranial magnetic stimulation. *Clin Neurophysiol* **124**, 1364-1372,
1100 (2013).

1101 75. Paulk, A. C., Zelmann, R., Crocker, B., Widge, A. S., Dougherty, D. D., Eskandar, E. N.,
1102 Weisholtz, D. S., Richardson, R. M., Cosgrove, G. R., Williams, Z. M. & Cash, S. S.
1103 Local and distant cortical responses to single pulse intracranial stimulation in the human
1104 brain are differentially modulated by specific stimulation parameters. *Brain Stimul* **15**,
1105 491-508, (2022).
1106 76. Huang, Y., Zelmann, R., Hadar, P., Dezha-Peralta, J., Richardson, R. M., Williams, Z. M.,
1107 Cash, S. S., Keller, C. J. & Paulk, A. C. Theta-burst direct electrical stimulation remodels
1108 human brain networks. *Nat Commun* **15**, 6982, (2024).
1109 77. Murphy, K. R. *et al.* Optimized ultrasound neuromodulation for non-invasive control of
1110 behavior and physiology. *Neuron*, (2024).
1111 78. Bures, J. & Buresova, O. Cerebral [K+]e increase as an index of the differential susceptibility
1112 of brain structures to terminal anoxia and electroconvulsive shock. *J Neurobiol* **12**, 211-
1113 220, (1981).
1114 79. Deluca, A. M., Pivik, R. T. & Chorover, S. L. Electroconvulsive shock: effects on sleep and
1115 cortical steady potential in the rat. *Physiol Behav* **18**, 997-1003, (1977).
1116 80. Rebert, C. S., Pryor, G. T. & Schaeffer, J. A. Slow cortical potential consequences of
1117 elctroconvulsive shock in rats. *Physiol Behav* **12**, 131-134, (1974).
1118 81. Moulier, V., Guehl, J., Eveque-Mourroux, E., Quesada, P. & Rotharmel, M. A Retrospective
1119 Study of Postictal Suppression during Electroconvulsive Therapy. *J Clin Med* **11**, (2022).
1120 82. J, C. M. P., J, P. A. J. V., Stuiver, S., Aalbregt, E., Schmettow, M., Hofmeijer, J., van
1121 Waarde, J. A. & M, J. A. M. v. P. Seizure duration predicts postictal
1122 electroencephalographic recovery after electroconvulsive therapy-induced seizures. *Clin*
1123 *Neurophysiol* **148**, 1-8, (2023).
1124 83. Hickman, L. B., Kafashan, M., Labonte, A. K., Chan, C. W., Huels, E. R., Guay, C. S., Guan,
1125 M. J., Ching, S., Lenze, E. J., Farber, N. B., Avidan, M. S., Hogan, R. E. & Palanca, B. J.
1126 A. Postictal generalized electroencephalographic suppression following electroconvulsive
1127 therapy: Temporal characteristics and impact of anesthetic regimen. *Clin Neurophysiol*
1128 **132**, 977-983, (2021).
1129 84. Pottkamper, J. C. M., Verdijk, J., Aalbregt, E., Stuiver, S., van de Mortel, L., Norris, D. G.,
1130 van Putten, M., Hofmeijer, J., van Wingen, G. A. & van Waarde, J. A. Changes in
1131 postictal cerebral perfusion are related to the duration of electroconvulsive therapy-
1132 induced seizures. *Epilepsia* **65**, 177-189, (2024).
1133 85. Hirano, J., Takamiya, A., Yamagata, B., Hotta, S., Miyasaka, Y., Pu, S., Iwanami, A.,
1134 Uchida, H. & Mimura, M. Frontal and temporal cortical functional recovery after
1135 electroconvulsive therapy for depression: A longitudinal functional near-infrared
1136 spectroscopy study. *J Psychiatr Res* **91**, 26-35, (2017).
1137 86. Downey, D., Brigadoi, S., Trevithick, L., Elliott, R., Elwell, C., McAllister-Williams, R. H.
1138 & Anderson, I. M. Frontal haemodynamic responses in depression and the effect of
1139 electroconvulsive therapy. *J Psychopharmacol* **33**, 1003-1014, (2019).
1140 87. Mulders, P. C. R. *et al.* Structural changes induced by electroconvulsive therapy are
1141 associated with clinical outcome. *Brain Stimul* **13**, 696-704, (2020).
1142 88. Verdijk, J. *et al.* Longitudinal resting-state network connectivity changes in
1143 electroconvulsive therapy patients compared to healthy controls. *Brain Stimul* **17**, 140-
1144 147, (2024).

1145 89. Abbott, C. C., Jones, T., Lemke, N. T., Gallegos, P., McClintock, S. M., Mayer, A. R.,
1146 Bustillo, J. & Calhoun, V. D. Hippocampal structural and functional changes associated
1147 with electroconvulsive therapy response. *Transl Psychiatry* **4**, e483, (2014).
1148 90. Argyelan, M. *et al.* Electric field causes volumetric changes in the human brain. *Elife* **8**,
1149 (2019).
1150 91. Cano, M., Lee, E., Cardoner, N., Martinez-Zalacain, I., Pujol, J., Makris, N., Henry, M., Via,
1151 E., Hernandez-Ribas, R., Contreras-Rodriguez, O., Menchon, J. M., Urretavizcaya, M.,
1152 Soriano-Mas, C. & Camprodon, J. A. Brain Volumetric Correlates of Right Unilateral
1153 Versus Bitemporal Electroconvulsive Therapy for Treatment-Resistant Depression. *J*
1154 *Neuropsychiatry Clin Neurosci* **31**, 152-158, (2019).
1155 92. Leaver, A. M., Vasavada, M., Kubicki, A., Wade, B., Loureiro, J., Hellemann, G., Joshi, S.
1156 H., Woods, R. P., Espinoza, R. & Narr, K. L. Hippocampal subregions and networks
1157 linked with antidepressant response to electroconvulsive therapy. *Mol Psychiatry* **26**,
1158 4288-4299, (2021).
1159 93. Drenckhahn, C., Winkler, M. K., Major, S., Scheel, M., Kang, E. J., Pinczolits, A., Grozea,
1160 C., Hartings, J. A., Woitzik, J., Dreier, J. P. & group, C. s. Correlates of spreading
1161 depolarization in human scalp electroencephalography. *Brain* **135**, 853-868, (2012).
1162 94. Thomas, R., Shin, S. S. & Balu, R. Applications of near-infrared spectroscopy in
1163 neurocritical care. *Neurophotonics* **10**, 023522, (2023).
1164 95. Lemale, C. L., Luckl, J., Horst, V., Reiffurth, C., Major, S., Hecht, N., Woitzik, J. & Dreier,
1165 J. P. Migraine Aura, Transient Ischemic Attacks, Stroke, and Dying of the Brain Share
1166 the Same Key Pathophysiological Process in Neurons Driven by Gibbs-Donnan Forces,
1167 Namely Spreading Depolarization. *Front Cell Neurosci* **16**, 837650, (2022).
1168 96. Hadjikhani, N., Sanchez Del Rio, M., Wu, O., Schwartz, D., Bakker, D., Fischl, B., Kwong,
1169 K. K., Cutrer, F. M., Rosen, B. R., Tootell, R. B., Sorensen, A. G. & Moskowitz, M. A.
1170 Mechanisms of migraine aura revealed by functional MRI in human visual cortex. *Proc*
1171 *Natl Acad Sci U S A* **98**, 4687-4692, (2001).
1172 97. Woods, R. P., Iacoboni, M. & Mazziotta, J. C. Brief report: bilateral spreading cerebral
1173 hypoperfusion during spontaneous migraine headache. *N Engl J Med* **331**, 1689-1692,
1174 (1994).
1175 98. Theilmann, W., Loscher, W., Socala, K., Frieling, H., Bleich, S. & Brandt, C. A new method
1176 to model electroconvulsive therapy in rats with increased construct validity and enhanced
1177 translational value. *J Psychiatr Res* **53**, 94-98, (2014).
1178 99. Vöröslakos, M., Takeuchi, Y., Brinyiczki, K., Zombori, T., Oliva, A., Fernández-Ruiz, A.,
1179 Kozák, G., Kincses, Z. T., Iványi, B., Buzsáki, G. & Berényi, A. Direct effects of
1180 transcranial electric stimulation on brain circuits in rats and humans. *Nature*
1181 *Communications* **9**, (2018).
1182 100. Su, Y., Radman, T., Vaynshteyn, J., Parra, L. C. & Bikson, M. Effects of high-frequency
1183 stimulation on epileptiform activity in vitro: ON/OFF control paradigm. *Epilepsia* **49**,
1184 1586-1593, (2008).
1185 101. Turner, D. A., Degan, S., Galeffi, F., Schmidt, S. & Peterchev, A. V. Rapid, Dose-
1186 Dependent Enhancement of Cerebral Blood Flow by transcranial AC Stimulation in
1187 Mouse. *Brain Stimul* **14**, 80-87, (2021).
1188 102. Abbott, C. C. *et al.* Amplitude-determined seizure-threshold, electric field modeling, and
1189 electroconvulsive therapy antidepressant and cognitive outcomes.
1190 *Neuropsychopharmacology* **49**, 640-648, (2024).

1191